

A. L. J. BURGMANS



THE TEMPERATURE AND CONCENTRATION
DEPENDENCE OF THE VISCOMAGNETIC
EFFECT

1872

1873

THE TEMPERATURE AND
CONCENTRATION DEPENDENCE
OF THE VISCOMAGNETIC

THE TEMPERATURE AND
CONCENTRATION DEPENDENCE
OF THE VISCOMAGNETIC
EFFECT

PROFSCHRIFT

TER VERKRIJFING VAN DE GRAAD VAN DOCTOR
IN DE WISSENSCHAPPE EN NATUURWETENSCHAPPEN
AAN DE RIJSDIVERSITEIT VAN LEIDEN OP DRAG
VAN DE SECTIE MAGNETIEKE DE A. N. CLAREN,
HOOGLERAAR IN DE FACULTEIT DER LETTEREN,
WEGENS BESLUIT VAN HET COLLEGE VAN
DOCTOREN TE VERDIENEN OP WOENSDAG
25 SEPTEMBER 1942 TE LEIDEN 13 13 1942

DOOR

ADRIANUS LEONARDUS JOSEPHUS PURGHANUS
GEBOREN TE OUDHOORN IN 1907

1942

INTERNATIONAL LIBRARY OF SCIENCE AND TECHNOLOGY

THE TEMPERATURE AND
CONCENTRATION DEPENDENCE
OF THE VISCOMAGNETIC
EFFECT

Cover picture: Leiden as seen from the Kamerlingh Onnes Laboratory.

THE TEMPERATURE AND
CONCENTRATION DEPENDENCE
OF THE VISCOMAGNETIC
EFFECT

PROEFSCHRIFT

TER VERKRIJGING VAN DE GRAAD VAN DOCTOR
IN DE WISKUNDE EN NATUURWETENSCHAPPEN
AAN DE RIJKSUNIVERSITEIT VAN LEIDEN, OP GEZAG
VAN DE RECTOR MAGNIFICUS DR. A. E. COHEN,
HOGLERAAR IN DE FACULTEIT DER LETTEREN,
VOLGENS BESLUIT VAN HET COLLEGE VAN
DECANEN TE VERDEDIGEN OP WOENSDAG
20 SEPTEMBER 1972 TE KLOKKE 15.15 UUR

DOOR

ADRIANUS LEONARDUS JOSEPHUS BURGMANS
GEBOREN TE UDENHOUT IN 1945

1972

DRUKKERIJ J. H. PASMANS, 'S-GRAVENHAGE

THE TEMPERATURE AND
CONCENTRATION DEPENDENCE
OF THE VISCOMAGNETIC
EFFECT

Promotoren: DR. H.F.P. KNAAP

PROF. DR. J.J.M. BEENAKKER

PROEFSCHRIFT

TER VERKRIJGING VAN DE GRAAD VAN DOCTOR
IN DE WISKUNDE EN NATUURWETENSCHAPPEN
AAN DE RIJSCHE UNIVERSITEIT VAN LEIDEN OP GEZAG
VAN DE RECTOR MAGISTRUS DR. A. E. COHEN
HOOGLEERAAR IN DE FACULTEIT DER WETENSCHAPPEN
VOLGENS BESLUIT VAN HET COLLEGE VAN
DECANEN TE VERDIENEN OP ZONDAG
20 SEPTEMBER 1972 TE ELKREEK 11.15 UUR

DOOR

ADRIANUS LEONARDUS JOSEPHUS BURGEMANS
GEBOREN TE UDENHOUT IN 1949

1972

DRUKKERIJ J. M. BAKKER, LEIDEN

CONTENTS

PREFACE

CHAPTER I. THE TEMPERATURE DEPENDENCE OF THE VICINEMAGNETIC EFFECT

1.	Introduction	11
2.	Experimental	13
2.1	Materials	13
2.2	Details	19
2.3	Consistency tests	27
3.	Calculation of the results	18
4.	Experimental results and discussion	29
5.	A comparison with nuclear magnetic resonance (N.M.R.) experiments	34
5.1	Survey of relaxation mechanisms	34
5.1.1	Spin-lattice relaxation	34
5.1.2	Spin-spin relaxation	36
5.1.3	Spin-rotation relaxation	37
5.2	Comparison of cross sections	38
5.2.1	Dihydrogen peroxide (D ₂)	39
5.2.2	Water (H ₂ O)	39
5.2.3	Methane (CH ₄)	39
5.2.4	Tetrahydrofuran (C ₄ H ₈ O)	39
5.2.5	Tetrahydrofuran (C ₄ H ₈ O)	40

Aan mijn ouders
Aan Francé

CHAPTER II. THE CONCENTRATION DEPENDENCY OF THE VICINEMAGNETIC EFFECT

1.	Introduction	41
2.	Experimental	42
2.1	Materials	42
2.2	Details	43
2.3	Consistency tests	44
3.	Calculation of the results	45
4.	Experimental results and discussion	46
4.1	Survey of relaxation mechanisms	46
4.1.1	Spin-lattice relaxation	46
4.1.2	Spin-spin relaxation	47
4.1.3	Spin-rotation relaxation	47
4.2	Comparison of cross sections	48
4.2.1	Dihydrogen peroxide (D ₂)	48
4.2.2	Water (H ₂ O)	48
4.2.3	Methane (CH ₄)	48
4.2.4	Tetrahydrofuran (C ₄ H ₈ O)	48
4.2.5	Tetrahydrofuran (C ₄ H ₈ O)	49

Proefschrift: DR. H.F.P. DE VRIES

PROF. DR. J.J.M. BEERMAN

van de

Stichting

Het in dit proefschrift beschreven onderzoek werd uitgevoerd als onderdeel van het programma van de werkgemeenschap voor Molecuulfysica van de Stichting voor Fundamenteel Onderzoek der Materie (F.O.M.) met financiële steun van de Nederlandse Organisatie voor Zuiver Wetenschappelijk Onderzoek (Z.W.O.).

CONTENTS

PREFACE	9
CHAPTER I. THE TEMPERATURE DEPENDENCE OF THE VISCOMAGNETIC EFFECT	11
1. Introduction	11
2. Experimental	13
2.1 General	13
2.2 Details	15
2.3 Consistency tests	17
3. Calculation of the results	18
4. Experimental results and discussion	20
5. A comparison with nuclear magnetic relaxation (N.M.R.) experiments	34
5.1 Survey of relaxation mechanisms	34
Diatomic molecules	34
Multilevel system	36
Spherical top molecules	37
5.2 Comparison of cross sections	38
Hydrogen deuteride (HD)	39
Nitrogen (N ₂)	39
Methane (CH ₄)	39
Tetrafluoromethane (CF ₄)	39
Tetradeuteromethane (CD ₄)	40
CHAPTER II. THE CONCENTRATION DEPENDENCE OF THE VISCOMAGNETIC EFFECT	45
1. Introduction	45
2. Theory	46
2.1 Position of the effect on the H/p axis	46
2.2 The magnitude of the field effect	49
3. Experiment	50

4. Experimental results and discussion	55
4.1 The $(H/p)_{1/2}$ value as a function of composition	56
4.2 The saturation value as a function of composition	63

SAMENVATTING	72
--------------	----

CURRICULUM VITAE	74
------------------	----

CHAPTER I. THE TEMPERATURE DEPENDENCE OF THE VISCOELASTIC PROPERTIES

11	1. Introduction	11
12	2. Experimental	12
13	2.1 General	13
14	2.2 Details	14
15	2.3 Complementary tests	15
16	3. Calculation of the results	16
17	4. Experimental results and discussion	17
18	5. A comparison with polymer magnetic relaxation (M.W.R.) experiments	18
19	5.1 Survey of relaxation mechanisms	19
20	5.1.1 Organic molecules	20
21	5.1.2 Cellulose system	21
22	5.1.3 Synthetic top molecules	22
23	5.2 Comparison of cross sections	23
24	Hydrogen (H ₂)	24
25	Nitrogen (N ₂)	25
26	Hydrogen cyanide (HCN)	26
27	Tetrafluoroethane (C ₂ F ₄)	27
28	Tetrahydrofuran (C ₄ H ₈ O)	28

CHAPTER II. THE DEPENDENCE OF THE VISCOELASTIC PROPERTIES ON THE CONCENTRATION OF THE VISCOELASTIC COMPONENT

29	1. Introduction	29
30	2. Experimental	30
31	2.1 General	31
32	2.2 Details	32
33	2.3 Complementary tests	33
34	3. Calculation of the results	34
35	4. Experimental results and discussion	35
36	5. A comparison with polymer magnetic relaxation (M.W.R.) experiments	36
37	5.1 Survey of relaxation mechanisms	37
38	5.1.1 Organic molecules	38
39	5.1.2 Cellulose system	39
40	5.1.3 Synthetic top molecules	40
41	5.2 Comparison of cross sections	41
42	Hydrogen (H ₂)	42
43	Nitrogen (N ₂)	43
44	Hydrogen cyanide (HCN)	44
45	Tetrafluoroethane (C ₂ F ₄)	45
46	Tetrahydrofuran (C ₄ H ₈ O)	46

Both chapters of this thesis will appear in Physica.

PREFACE

In the presence of a gradient in a macroscopic quantity (temperature or bulk velocity) in a gas, the spacial distribution of the peculiar velocities \underline{W} of the molecules is no longer isotropic. For a noble gas, such a polarization in velocity space is responsible for the transport of energy or momentum. The situation is more complicated for a gas of polyatomic molecules. In this case, collisions can induce polarizations involving the direction of the angular momentum \underline{J} of the molecules. A gradient in the bulk velocity (viscosity experiments) produces a polarization in \underline{W} space of the quadrupole type $\langle [\underline{W}]^{(2)} \rangle$ and this produces a polarization of the angular momenta of the type $\langle [\underline{J}]^{(2)} \rangle$.

On application of an external magnetic field the angular momenta begin to precess around the field direction partially destroying the $\langle [\underline{J}]^{(2)} \rangle$ polarization. This in turn decreases the polarization in velocities thus changing the viscosity coefficient (viscomagnetic effect). From this change, information can be obtained about the strength of the coupling between the anisotropies in \underline{W} and \underline{J} space and about the decay time of the $\langle [\underline{J}]^{(2)} \rangle$ polarization. Both these quantities are determined mainly by the non-spherical part of the intermolecular potential. A study of the field effect therefore affords the possibility of probing the non-spherical part of the molecular interaction.

When the present research was initiated nearly all experiments on the viscomagnetic effect were performed at room temperature. It is necessary, however, to have data over a large temperature range in order to obtain significant information on the molecular interaction. For this reason the field effect on viscosity at different temperatures has been investigated. In chapter I the results are presented for HD, N_2 , CO and CH_4 for temperatures ranging from 293 K down to about the boiling point of these gases.

Another source of information on the decay of polarizations in \underline{J} space is given by nuclear magnetic relaxation (NMR) measurements in dilute gases. In chapter I section 5 a detailed comparison is made between

results obtained from the viscomagnetic effect and those from NMR for the gases HD, N₂, CH₄, CF₄ and CD₄.

The description of the interaction between two polyatomic molecules is complicated. Hence it is useful to consider the more simple case of the interaction between a polyatomic molecule and a noble gas atom. For this purpose binary mixtures of polyatomic gases and noble gases have been studied. In chapter II results are presented which have been obtained for the systems HD-He, HD-Ne, HD-Ar, N₂-He, N₂-Ne and N₂-Ar at both 77 K and 293 K.

CHAPTER I

THE TEMPERATURE DEPENDENCE OF THE
VISCOMAGNETIC EFFECT

1. *Introduction.* It is well known that the viscosity of polyatomic gases is influenced by a magnetic field^{1,2)}. An explanation of this field effect on dilute polyatomic gases can be given as follows. A velocity gradient in a gas of non-spherical molecules gives rise to an anisotropy not only in the velocities, \underline{W} , but also through collisions in the angular momenta, \underline{J} . This polarization (actually alignment) in the angular momenta can be partially destroyed by the action of a magnetic field (through the Larmor precession). This decreases the polarization in the velocities which changes the transport coefficients.

To describe the viscous behaviour of an isotropic fluid in a magnetic field five shear viscosity coefficients are needed. Until recently the notation used was that of refs. 3 and 4 where η_1 to η_5 were introduced. As this enumeration is not very expressive we prefer the notation which is introduced by Coope and Snider⁵⁾. They use the elements η_0^+ , η_1^+ , η_2^+ , η_1^- and η_2^- of the real spherical viscosity tensor given by (field in the z direction):

$$\begin{bmatrix}
 \left(\frac{3}{2}\right)^{1/2} [\underline{\Pi}]_{zz}^{(2)} \\
 [\underline{\Pi}]_{xz}^{(2)} \\
 [\underline{\Pi}]_{yz}^{(2)} \\
 \frac{1}{2} ([\underline{\Pi}]_{xx}^{(2)} - [\underline{\Pi}]_{yy}^{(2)}) \\
 [\underline{\Pi}]_{xy}^{(2)}
 \end{bmatrix}
 = -2
 \begin{bmatrix}
 \eta_0^+ & 0 & 0 & 0 & 0 \\
 0 & \eta_1^+ & -\eta_1^- & 0 & 0 \\
 0 & \eta_1^- & \eta_1^+ & 0 & 0 \\
 0 & 0 & 0 & \eta_2^+ & -\eta_2^- \\
 0 & 0 & 0 & \eta_2^- & \eta_2^+
 \end{bmatrix}
 \begin{bmatrix}
 \left(\frac{3}{2}\right)^{1/2} [\underline{v}]_{zz}^{(2)} \\
 [\underline{v}]_{xz}^{(2)} \\
 [\underline{v}]_{yz}^{(2)} \\
 \frac{1}{2} ([\underline{v}]_{xx}^{(2)} - [\underline{v}]_{yy}^{(2)}) \\
 [\underline{v}]_{xy}^{(2)}
 \end{bmatrix}
 \quad (1)$$

where $[\Pi]_{kl}^{(2)}$ are elements of the symmetric traceless pressure tensor and $[\underline{v}v]_{kl}^{(2)}$ are elements of the symmetric traceless velocity gradient tensor. The coefficients with a + sign are even, those with a - sign odd functions of the magnetic field. The subscripts 0, 1, 2 refer to the symmetry character of the particular velocity gradients under rotations around the field direction. This notation is also closely related to the notation of Hess and Waldmann⁶⁾. In table I we summarize the relations between the different notations.

TABLE I

Identification of the viscosity coefficients as used by different authors.

Coope and Snider ⁵⁾	De Groot and Mazur ⁴⁾	Hess and Waldmann ⁶⁾
η_0^+	η_1	$\eta^{(0)}$
η_1^+	η_3	Re $\eta^{(1)}$
η_2^-	$2\eta_2 - \eta_1$	Re $\eta^{(2)}$
η_1^-	η_5	Im $\eta^{(1)}$
η_2^-	$-\eta_4$	Im $\eta^{(2)}$

Experimentally it has been shown by Hulsman *et al.*⁷⁻⁹⁾ that for most simple gases the field effect can be described for all five coefficients by the presence of one type of angular momentum polarization, *viz.* $[J]^{(2)}$. In this case the experimental results can be characterized by two parameters, one describing the magnitude of the viscosity change and one characterizing the field strength at which the effect occurs. These quantities are related to collision integrals, thus providing direct information on the collisional processes. In particular, the collision integrals obtained are mainly determined by the non-spherical part of the intermolecular interaction.

Up to now nearly all experiments have been performed at room temperature. For a meaningful test of non-spherical potentials it would be very useful to know the temperature dependence of the collision integrals. In the present work such results are given for HD, N₂, CO and CH₄ for temperatures ranging from room temperature down to about the boiling point of these gases.

The results will furthermore be compared with measurements of nuclear magnetic relaxation since these experiments give information concerning the reorientation of the molecules which is similar to that obtained from our experiments.

2. *Experimental.* 2.1 *General.* As the field effect originates from one type of angular momentum polarization only, the two parameters characterizing the situation can be obtained from any combination of the coefficients η_1^+ , η_2^+ , η_1^- and η_2^- . Hence the choice of the coefficients to be measured can be determined on the basis of experimental convenience. We use two apparatuses, one (apparatus I) for measurements above 77 K and one (apparatus II) for lower temperatures. Both apparatuses can be considered as a Wheatstone bridge for gasflow, where the resistors are capillaries.

Apparatus I is of the same type as that used by Korving *et al.*¹⁰⁾. A capillary of circular cross section (capillary #1 in fig. 1) is placed between the poles of a magnet perpendicular to the field direction while the other capillaries are outside the field. On application of the field the viscosity of the gas in the in-field-capillary changes and consequently there is a change in the pressure drop over the capillary. This causes an unbalance of the bridge which is measured with manometer M. From this unbalance one can obtain the viscosity change given by (see also ref. 10):

$$\frac{1}{2} [\eta_1^+ + \eta_2^+ - 2\eta(0)] \quad (2)$$

where $\eta(0)$ is the field free viscosity coefficient.

In apparatus II all four capillaries of the bridge are placed in the field *i.e.*, two parallel and two perpendicular to the field direction

(see fig. 2). Since the combination of coefficients measured in a capillary parallel to the field is different from that measured in a capillary perpendicular to the field, a net effect will result given by (see also ref. 11):

$$\frac{1}{2} (-\eta_1^+ + \eta_2^+). \quad (3)$$

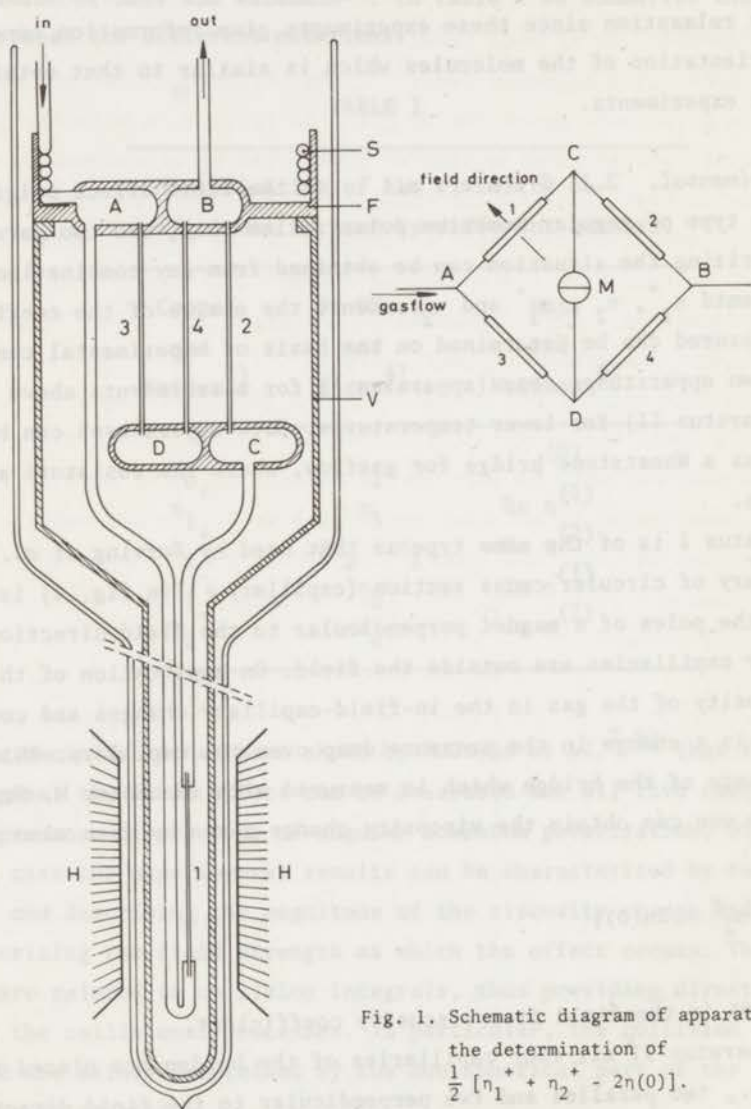


Fig. 1. Schematic diagram of apparatus I for the determination of $\frac{1}{2} [\eta_1^+ + \eta_2^+ - 2\eta(0)]$.

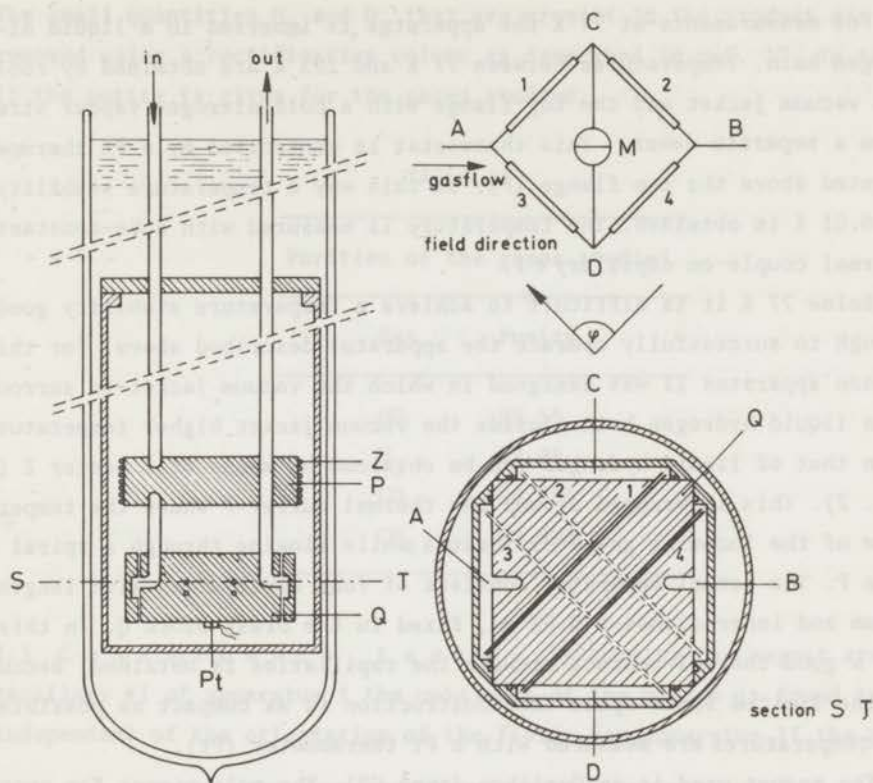


Fig. 2. Schematic diagram of apparatus II for the determination of $\frac{1}{2}(-\eta_1^* + \eta_2^*)$.

2.2 Details. From earlier room temperature work⁷⁻¹¹⁾ it became clear that to obtain a sufficiently constant gasflow through the bridge a good temperature stability is required. Thus it proved necessary to isolate the capillaries by means of a vacuum jacket. In apparatus I this vacuum jacket (V) is quite long (about one meter), which makes it possible to have one capillary in the field and the three others outside the field (see fig. 1). The part of the apparatus inside the vacuum jacket is in thermal contact with the environment through the top flange (F) that also acts as a thermal buffer. The incoming gas is brought to thermal equilibrium in the spiral S, while the volumes A, B, C and D damp out fluctuations in the gasflow. The in-field-capillary has a length of 113 mm and an inner diameter of 1.2 mm.

For measurements at 77 K the apparatus is immersed in a liquid nitrogen bath. Temperatures between 77 K and 293 K are obtained by cooling the vacuum jacket and the top flange with a cold nitrogen vapour stream from a separate dewar. This thermostat is controlled by a Pt thermometer mounted above the top flange (F). In this way a temperature stability of 0.01 K is obtained. The temperature is measured with a Fe-constantan thermal couple on capillary # 1.

Below 77 K it is difficult to achieve a temperature stability good enough to successfully operate the apparatus described above. For this reason apparatus II was designed in which the vacuum jacket is surrounded by a liquid hydrogen bath. Inside the vacuum jacket higher temperatures than that of liquid hydrogen can be obtained by means of a heater Z (see fig. 2). This is wrapped around the thermal buffer P where the temperature of the incoming gas equilibrates while flowing through a spiral inside P. The actual apparatus consists of four capillaries with length 75 mm and inner diameter 0.63 mm, fixed in the brass block Q. In this way a good thermal contact between the capillaries is obtained. Because of the limited field space the construction is as compact as possible. The temperatures are measured with a Pt thermometer (Pt).

The magnet used is an Oerlikon (type C3). The pole pieces for apparatus I have a diameter of 120 mm. With a distance of 50 mm a maximum field of 31.5 kOe can be reached. For apparatus II the maximum field is limited to 22.6 kOe since in that case pole pieces are used of 180 mm diameter at a distance of 120 mm.

In both apparatuses the gasflow through the bridge is adjusted by means of a needle valve upstream and is kept constant by a flow controller (Moore 63 BDL). The pressure in the capillaries can be varied by a valve at the exit of the bridge. The pressures at the points A, B and C are measured with oil manometers. The unbalance of the bridge is measured with a differential membrane manometer with a sensitivity of 10^{-5} torr (Varian MMM).

The gases used are obtained commercially except HD which is prepared using the reaction:



The small quantities H_2 and D_2 that are present in the product gas are removed using a rectification column as described in ref. 12. In table II the purity is given for the gases studied.

TABLE II

Purities of the gases studied

Gas	Purity
HD	99.5%
N_2	99.9%
CO	99.95%
CH_4	99.99%

2.3 Consistency tests. By turning the magnet around capillary #1 of apparatus I the unbalance of the bridge is found to be independent of the orientation of the field. For apparatus II the pres-

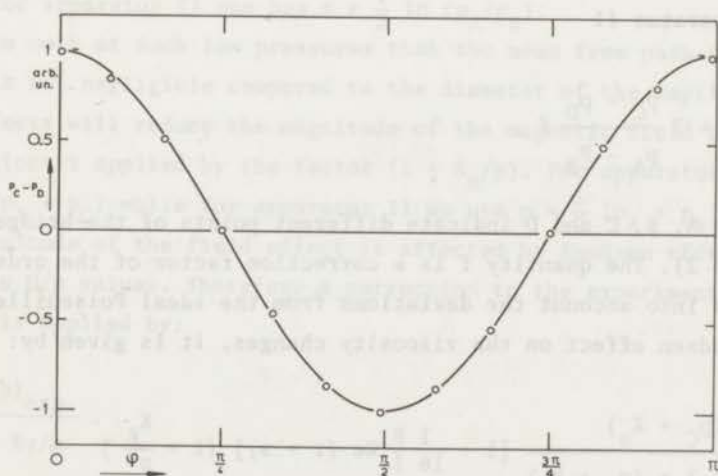


Fig. 3. The normalized pressure difference $p_C - p_D$ which arises in apparatus II versus the orientation of the magnetic field with respect to the capillaries. The solid line is given by $\cos 2\phi$ where ϕ is the angle in fig. 2.

sure difference $p_C - p_D$ is a function of the angle ϕ (see fig. 2) between the field direction and the direction of one set of capillaries. The dependence of $p_C - p_D$ on ϕ can be derived from the equations of motion given in ref. 13 and it is found that:

$$p_C - p_D = (p_C - p_D)_{\phi=0} \cos 2\phi. \quad (4)$$

Indeed measurements on a test gas (N_2) as a function of ϕ can be described by eq. (4) which is illustrated in fig. 3.

Performing experiments with noble gases, no effect could be detected, as should be expected.

3. *Calculation of the results.* In both apparatuses the pressure difference $p_C - p_D$ across the bridge is measured which arises on application of the field. For apparatus I the field effects are calculated with:

$$\frac{\eta_1^+ + \eta_2^+ - 2\eta(0)}{2\eta(0)} = 4 \frac{p_C - p_D}{p_A - p_B} f \quad (5)$$

and for apparatus II

$$\frac{-\eta_1^+ + \eta_2^+}{2\eta(0)} = 2 \frac{p_C - p_D}{p_A - p_B} f. \quad (6)$$

The indices A, B, C and D indicate different points of the bridge (see figs. 1 and 2). The quantity f is a correction factor of the order unity which takes into account the deviations from the ideal Poiseuille flow and the Knudsen effect on the viscosity changes. It is given by:

$$f = \frac{2(p_C + K_\alpha)}{(p_A + K_\alpha) + (p_B + K_\alpha)} \left[1 + \frac{1}{16} \frac{R}{l} \operatorname{Re}(r + s) \right] \left(1 + \frac{K_\beta}{p} \right) \quad (7)$$

(see also refs. 8 and 11).

The factor $2(p_C + K_\alpha)/[(p_A + K_\alpha) + (p_B + K_\alpha)]$ takes into account the

expansion of the gas. For apparatus I the expansion factor is usually around 1.3 while for apparatus II this factor is always between 1 and 1.03. The quantity K_α gives the Knudsen correction for the field free flow and can be written as $K_\alpha = n_\alpha p \xi/R$, where R is the radius of the capillary, ξ the mean free path of the molecules given by $\xi = (2^{1/2} n \sigma^2)^{-1}$ with n the number density and σ the molecular diameter derived from the field free viscosity, given in ref. 14. In accordance with refs. 15 and 16 it is assumed that n_α has the value 4.

The second factor in eq. (7) corrects for the extra pressure losses caused by acceleration of the gas at the entrance of the capillary and in the capillary. For both apparatuses this factor is mostly between 1 and 1.01. Here l is the length of the capillary and Re is Reynolds number equal to $2G/\pi R \eta(0)$ where G is the massflow per unit time through the capillary. The quantity r depends on the shape of the entrance and in accordance with ref. 15 r is assumed to be 1. The quantity s describes the acceleration of the gas in the capillary. For the two apparatuses s is slightly different since in apparatus I only one capillary is in the field while in apparatus II this is the case for all four capillaries. Consequently for apparatus I the quantity s is given by $s = \ln(p_A/p_C)$ while for apparatus II one has $s = \frac{1}{2} \ln(p_A/p_B)$.

As we work at such low pressures that the mean free path of the molecules is not negligible compared to the diameter of the capillaries, Knudsen effects will reduce the magnitude of the magnetic field effects. A correction is applied by the factor $(1 + K_\beta/p)$. For apparatus I we take $p = \frac{1}{2}(p_A + p_C)$ while for apparatus II we use $p = \frac{1}{2}(p_A + p_B)$. Not only the magnitude of the field effect is affected by Knudsen effects but also the H/p values. Therefore a correction to the experimental H/p values is applied by:

$$\frac{H}{P} = \frac{(H/p)_{\text{exp.}}}{1 + K_Y/p} \quad (8)$$

The quantities K_β and K_Y are determined experimentally from an extrapolation to $p = \infty$. For a more detailed discussion see ref. 8. The correction factor for the magnitude of the effect is at most 1.4 while the

Knudsen correction for the H/p values is generally small except for HD where the correction factor can be as large as 1.3. Analogous to n_α the numbers n_β and n_γ can be introduced⁸⁾ by: $K_{\beta,\gamma} = n_{\beta,\gamma} p\xi/R$. Within the experimental accuracy these numbers are found to be independent of the temperature and also equal for the two apparatuses. The values found for the different gases are presented in table III. The values are in agreement with those obtained in the earlier room temperature measurements^{8,9)}.

TABLE III

Knudsen correction parameters			
	n_α	n_β	n_γ
HD	4	10	14
N ₂	4	10	3
CO	4	10	3
CH ₄	4	12	2

4. *Experimental results and discussion.* To discuss the experimental results we first give the theoretical expressions derived in ref. 17 for $[\eta_1^+ + \eta_2^+ - 2\eta(0)]/2\eta(0)$ and $(-\eta_1^+ + \eta_2^+)/2\eta(0)$ based on the $[J]^{(2)}$ polarization which in earlier experiments is found to be dominant:

$$\frac{\eta_1^+ + \eta_2^+ - 2\eta(0)}{2\eta(0)} = -\frac{1}{2} \psi_{02} \left[\frac{\xi_{02}^2}{1 + \xi_{02}^2} + \frac{4\xi_{02}^2}{1 + 4\xi_{02}^2} \right] \quad (9)$$

and

$$\frac{-\eta_1^+ + \eta_2^+}{2\eta(0)} = -\frac{1}{2} \psi_{02} \left[-\frac{\xi_{02}^2}{1 + \xi_{02}^2} + \frac{4\xi_{02}^2}{1 + 4\xi_{02}^2} \right] \quad (10)$$

where

$$\Psi_{02} = \frac{\mathfrak{E}_{(20)}^{(02)2}}{\mathfrak{E}(20) \mathfrak{E}(02)}, \quad (11)$$

$$\xi_{02} = \frac{1}{\langle v_{\text{rel}} \rangle_0} \frac{g \mu_N kT}{\hbar} \frac{H}{P} \quad (12)$$

and

$$\eta(0) = \frac{kT}{\langle v_{\text{rel}} \rangle_0 \mathfrak{E}(20)} \quad (13)$$

g is the molecular g -factor, μ_N the nuclear magneton, k Boltzmann's constant, T the absolute temperature, \hbar Planck's constant and

$$\langle v_{\text{rel}} \rangle_0 = \left(\frac{8 kT}{\pi \mu} \right)^{1/2} \quad (14)$$

with μ the reduced mass. The \mathfrak{E} 's are effective cross sections* given by 19):

$$\begin{aligned} \mathfrak{E}(20) &= \frac{1}{\langle v_{\text{rel}} \rangle_0} \frac{\langle [W]^{(2)} : R_0 [W]^{(2)} \rangle_0}{\langle [W]^{(2)} : [W]^{(2)} \rangle_0}; \quad \mathfrak{E}(02) = \frac{1}{\langle v_{\text{rel}} \rangle_0} \frac{\langle [J]^{(2)} : R_0 [J]^{(2)} \rangle_0}{\langle [J]^{(2)} : [J]^{(2)} \rangle_0} \\ \mathfrak{E}_{(20)}^{(02)} &= \frac{1}{\langle v_{\text{rel}} \rangle_0} \frac{\langle [J]^{(2)} : R_0 [W]^{(2)} \rangle_0}{\langle [J]^{(2)} : [J]^{(2)} \rangle_0^{1/2} \langle [W]^{(2)} : [W]^{(2)} \rangle_0^{1/2}}. \end{aligned} \quad (15)$$

R_0 is the collision superoperator defined by:

$$\begin{aligned} R_0 \phi &= -(2\pi)^4 \hbar^2 n^{-1} \text{tr}_1 \int dp_1 f_1^{(0)} \{ \int t_g^g, (\phi' + \phi_1') t_g^g, \delta(E) dp' + \\ &- \frac{i}{2\pi} [t_g^g (\phi + \phi_1) - (\phi + \phi_1) t_g^g] \}. \end{aligned} \quad (16)$$

* The shorthand notations $\mathfrak{E}_{(20)}^{(02)}$, $\mathfrak{E}(02)$ and $\chi(20)$ corresponds to the full notations $\mathfrak{E}_{(2000)}^{(0200)}$, $\mathfrak{E}_{(0200)}^{(0200)}$ and $\mathfrak{E}_{(2000)}^{(2000)}$ in more detailed discussions (see *e.g.* table II in ref. 18 and the appendix of ref. 9).

For the meaning of the different symbols see for example ref. 20. $\mathfrak{E}(20)$ is the gas-kinetic viscosity cross section, $\mathfrak{E}(02)$ is the reorientation cross section for tensorial polarization of the rotational angular momentum and $\mathfrak{E}_{20}^{(02)}$ is the cross section which describes the production of the angular momentum polarization from the polarization in the velocities. While $\mathfrak{E}(20)$ and $\mathfrak{E}(02)$ are positive, $\mathfrak{E}_{20}^{(02)}$ can have either sign.

For HD the experimental results have been given for the quantities $[\eta_1^+ + \eta_2^+ - 2\eta(0)]/2\eta(0)$ and $(-\eta_1^+ + \eta_2^+)/2\eta(0)$ in the figs. 4 and 5.

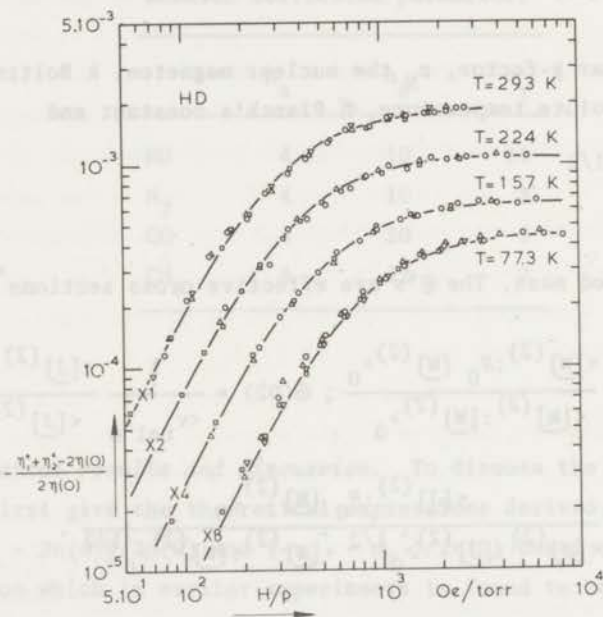


Fig. 4. $-\eta_1^+ + \eta_2^+ - 2\eta(0)/2\eta(0)$ versus H/p for HD at various temperatures.

To distinguish the four different curves for 293 K, 224 K, 157 K and 77.3 K, they are vertically shifted by dividing them respectively by 1, 2, 4 and 8.

77.3 K : \circ 3.48 torr; Δ 4.65 torr; ∇ 9.45 torr; \square 15.7 torr.

157 K : \circ 4.54 torr; Δ 6.44 torr; \square 10.5 torr.

224 K : \circ 4.58 torr; Δ 6.89 torr; \square 11.3 torr.

293 K : \circ 9.76 torr; Δ 12.4 torr; ∇ 15.6 torr; \square 20.8 torr.

— theoretical H/p dependence for $[J]^{(2)}$ polarization, scaled to the experimental points.

In these figures the theoretical curves are given by eqs. (9) and (10) with $\mathcal{E}(02)$ and $|\mathcal{E}(20)|$ as adaptable parameters, for the position along the H/p axis and the magnitude of the effect. It is seen that for both combinations of coefficients the experimental data can be described very well with the theoretical expressions based on the $[J]^{(2)}$ polarization only. At 77 K both combinations of coefficients have been measured. The

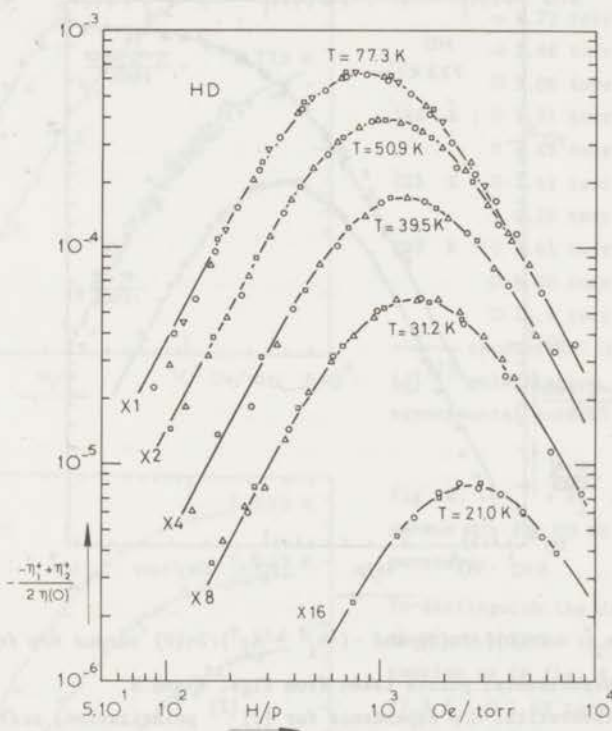


Fig. 5. $(-\eta_1^+ + \eta_2^+)/2\eta(0)$ versus H/p for HD at various temperatures.

To distinguish the different curves, they are shifted in the vertical direction as in fig. 4.

21.0 K : \square 1.49 torr; \square 2.95 torr.

31.2 K : \circ 1.89 torr; Δ 4.36 torr; \square 8.10 torr.

39.5 K : \circ 2.03 torr; Δ 4.04 torr; \square 7.78 torr.

50.9 K : \circ 2.03 torr; Δ 4.10 torr; \square 7.93 torr.

77.3 K : \circ 4.53 torr; Δ 4.79 torr; ∇ 6.71 torr; \square 12.2 torr.

— theoretical H/p dependence for $[J]^{(2)}$ polarization, scaled to the experimental points.

results from both apparatuses can be described using a single set of values of the adaptable parameters (see fig. 6). From these results we draw two main conclusions: a. the results obtained with apparatus I and with apparatus II are consistent within the experimental accuracy and b. the $[J]^{(2)}$ polarization is by far dominant for HD in the whole temperature region.

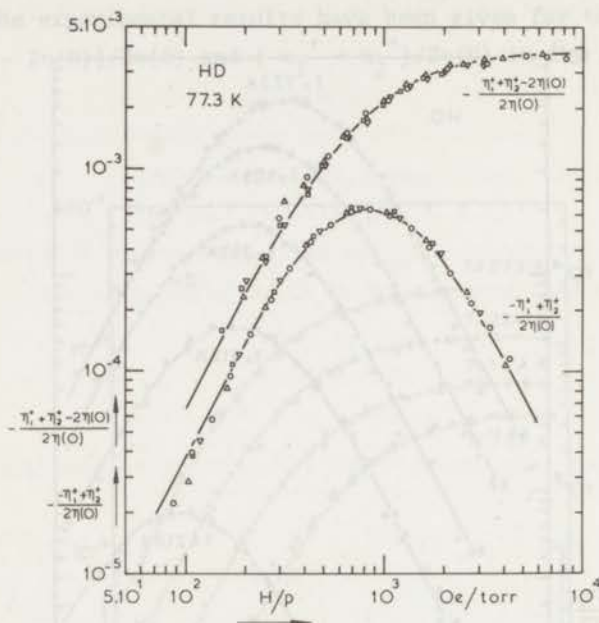


Fig. 6. $-\frac{[\eta_1^+ + \eta_2^+ - 2\eta(0)]}{2\eta(0)}$ and $\frac{-\eta_1^+ + \eta_2^+}{2\eta(0)}$ versus H/p for HD at 77.3 K.

$\circ \Delta \nabla \square$ experimental points taken from figs. 4 and 5.

— theoretical H/p dependence for $[J]^{(2)}$ polarization, scaled to the experimental points.

The results for $[\eta_1^+ + \eta_2^+ - 2\eta(0)]/2\eta(0)$ obtained at various temperatures for the gases N_2 , CO and CH_4 are given in figs. 7, 8 and 9. The theoretical curves have been given by eq. (9) with $\mathcal{E}(02)$ and $|\mathcal{E}_{20}^{02}|$ as adaptable parameters. It is seen that also here the experiments can be described with the theoretical expression. For N_2 and CO we also measured at 77 K the combination $(-\eta_1^+ + \eta_2^+)/2\eta(0)$. Here the results of the two experiments can also be described with one set of values

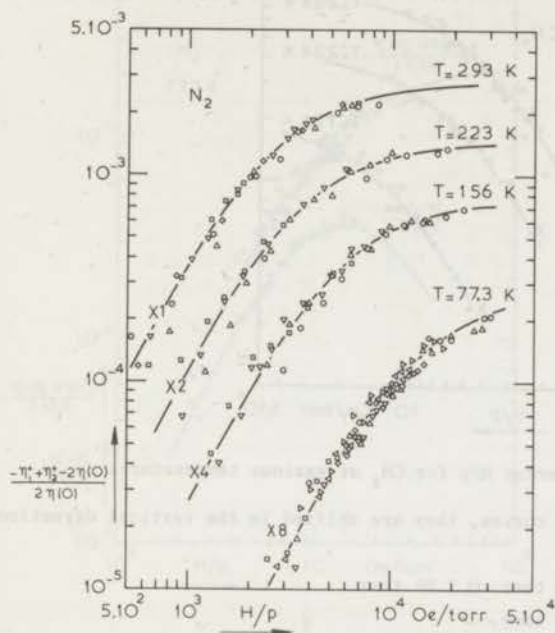


Fig. 7. $-[n_1^+ + n_2^+ - 2n(0)]/2n(0)$ versus H/p for N_2 at various temperatures.

To distinguish the different curves, they are shifted in the vertical direction as in fig. 4.

77.3 K : \circ 0.966 torr; Δ 1.09 torr;
 \triangleright 1.72 torr; \diamond 2.04 torr;
 \triangleleft 2.48 torr; ∇ 3.29 torr;
 \square 5.08 torr.

156 K : \circ 1.31 torr; Δ 1.96 torr;
 ∇ 3.43 torr; \square 4.95 torr.

223 K : \circ 1.61 torr; Δ 2.45 torr;
 ∇ 4.25 torr; \square 8.44 torr.

293 K : \circ 3.61 torr; Δ 4.60 torr;
 \diamond 5.39 torr; ∇ 7.61 torr;
 \square 15.5 torr.

— theoretical H/p dependence for $[J]^{(2)}$ polarization, scaled to the experimental points.

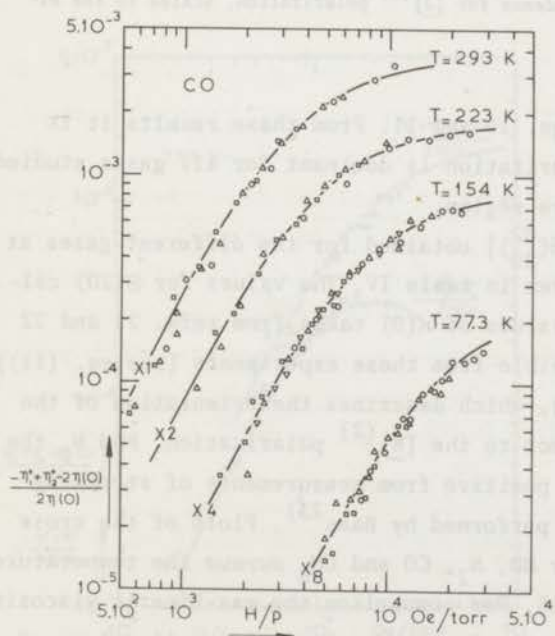


Fig. 8. $-[n_1^+ + n_2^+ - 2n(0)]/2n(0)$ versus H/p for CO at various temperatures.

To distinguish the different curves, they are shifted in the vertical direction as in fig. 4.

77.3 K : \circ 1.03 torr; Δ 1.53 torr;
 \square 2.49 torr.

154 K : \circ 1.32 torr; Δ 1.88 torr;
 ∇ 2.71 torr; \square 5.12 torr.

223 K : \circ 1.18 torr; Δ 2.54 torr;
 \square 4.38 torr.

293 K : \circ 2.89 torr; Δ 5.20 torr;
 \square 8.79 torr.

— theoretical H/p dependence for $[J]^{(2)}$ polarization, scaled to the experimental points.

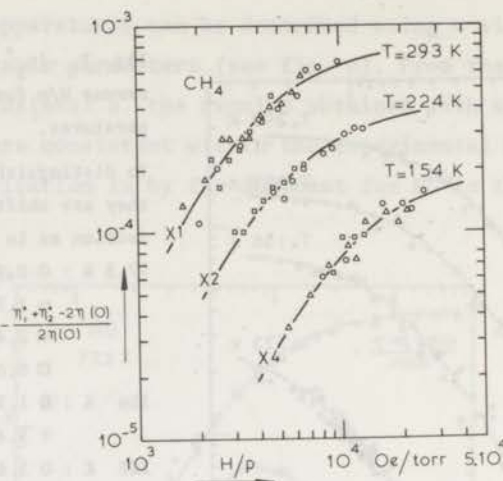


Fig. 9. $-\frac{[\eta_1^+ + \eta_2^+ - 2\eta(0)]}{2\eta(0)}$ versus H/p for CH_4 at various temperatures.

To distinguish the different curves, they are shifted in the vertical direction as in fig. 4.

154 K : \circ 0.904 torr; Δ 1.40 torr; \square 2.09 torr.

224 K : \circ 2.29 torr; \square 4.10 torr.

293 K : \circ 3.06 torr; Δ 4.71 torr; \square 6.78 torr.

— theoretical H/p dependence for $[J]^{(2)}$ polarization, scaled to the experimental points.

for $\mathfrak{E}(02)$ and $|\mathfrak{E}_{20}^{(02)}|$, see figs. 10 and 11. From these results it is concluded that the $[J]^{(2)}$ polarization is dominant for all gases studied in the investigated temperature region.

The parameters $\mathfrak{E}(02)$ and $|\mathfrak{E}_{20}^{(02)}|$ obtained for the different gases at different temperatures are given in table IV. The values for $\mathfrak{E}(20)$ calculated using the literature values of $\eta(0)$ taken from refs. 21 and 22 are also given. It is not possible from these experiments [see eq. (11)] to determine the sign of $\mathfrak{E}_{20}^{(02)}$, which describes the orientation of the $[J]^{(2)}$ polarization with respect to the $[W]^{(2)}$ polarization. For N_2 the sign of $\mathfrak{E}_{20}^{(02)}$ is found to be positive from measurements of streaming birefringence which have been performed by Baas²³. Plots of the cross sections $\mathfrak{E}(02)$ and $|\mathfrak{E}_{20}^{(02)}|$ for HD, N_2 , CO and CH_4 versus the temperature are given in the figs. 12 to 15. For comparison the gas-kinetic viscosity cross section $\mathfrak{E}(20)$ is also given. From the relatively small values of

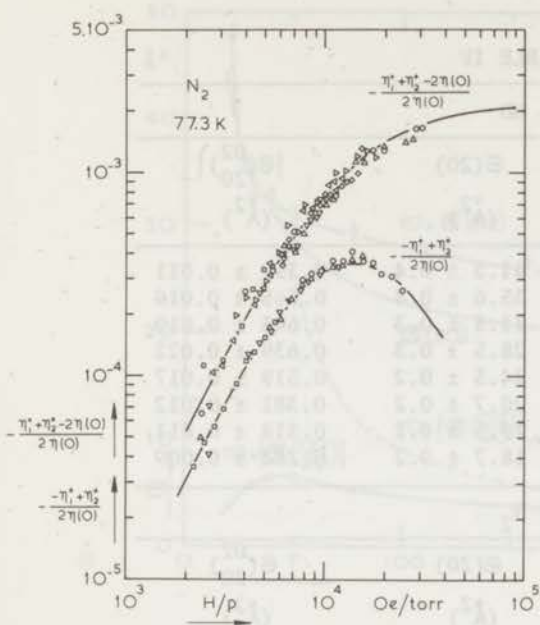


Fig. 10. $-\left[\eta_1^+ + \eta_2^+ - 2\eta(0)\right]/2\eta(0)$ and $-(\eta_1^+ + \eta_2^+)/2\eta(0)$ versus H/p for N_2 at 77.3 K.

upper curve: $\circ\Delta\triangleright\triangleleft\nabla\square$ points taken from fig. 7.

lower curve: \circ 0.829 torr; Δ 1.38 torr; ∇ 2.03 torr; \square 3.90 torr.

— theoretical H/p dependence for $[J]^{(2)}$ polarization, scaled to the experimental points.

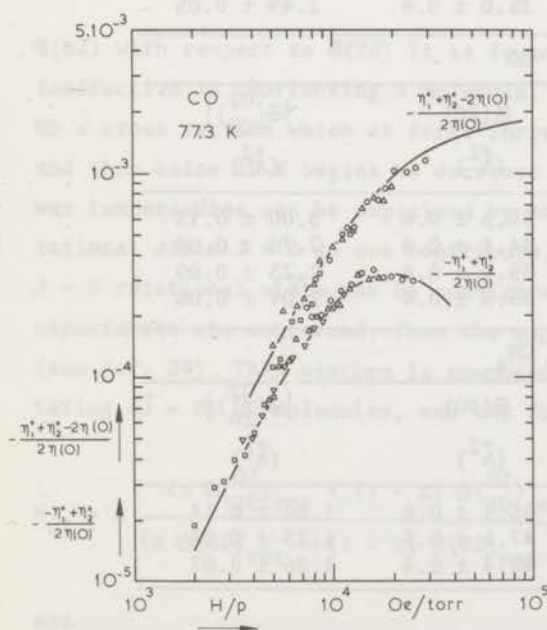


Fig. 11. $-\left[\eta_1^+ + \eta_2^+ - 2\eta(0)\right]/2\eta(0)$ and $-(\eta_1^+ + \eta_2^+)/2\eta(0)$ versus H/p for CO at 77.3 K.

upper curve: $\circ\Delta\square$ points taken from fig. 8.

lower curve: \circ 0.802 torr; Δ 1.22 torr; ∇ 1.89 torr; \square 4.33 torr.

— theoretical H/p dependence for $[J]^{(2)}$ polarization, scaled to the experimental points.

TABLE IV

HD			
T	$\epsilon(02)$	$\epsilon(20)$	$ \epsilon_{(20)}^{(02)} $
(K)	(\AA^2)	(\AA^2)	(\AA^2)
21.0	4.79 ± 0.09	41.3 ± 0.4	0.392 ± 0.011
31.2	3.26 ± 0.09	35.6 ± 0.4	0.565 ± 0.019
39.5	3.27 ± 0.07	31.5 ± 0.3	0.643 ± 0.019
50.9	3.09 ± 0.08	28.5 ± 0.3	0.639 ± 0.022
77.3	2.95 ± 0.08	24.5 ± 0.2	0.519 ± 0.017
157	2.67 ± 0.07	20.7 ± 0.2	0.381 ± 0.012
224	2.36 ± 0.07	19.5 ± 0.2	0.318 ± 0.011
293	2.26 ± 0.07	18.7 ± 0.2	0.282 ± 0.009
N_2			
T	$\epsilon(02)$	$\epsilon(20)$	$\epsilon_{(20)}^{(02)}$
(K)	(\AA^2)	(\AA^2)	(\AA^2)
77.3	61.9 ± 2.2	57.7 ± 0.6	2.77 ± 0.13
156	37.7 ± 1.9	42.6 ± 0.4	2.19 ± 0.10
223	27.8 ± 1.1	37.7 ± 0.4	1.71 ± 0.07
293	23.7 ± 0.9	35.0 ± 0.4	1.49 ± 0.05
CO			
T	$\epsilon(02)$	$\epsilon(20)$	$ \epsilon_{(20)}^{(02)} $
(K)	(\AA^2)	(\AA^2)	(\AA^2)
77.3	85.6 ± 3.2	55.3 ± 0.6	3.00 ± 0.13
154	50.1 ± 1.5	44.1 ± 0.4	2.70 ± 0.09
223	36.3 ± 1.5	39.1 ± 0.4	2.23 ± 0.09
293	32.5 ± 0.8	35.5 ± 0.4	2.04 ± 0.06
CH_4			
T	$\epsilon(02)$	$\epsilon(20)$	$ \epsilon_{(20)}^{(02)} $
(K)	(\AA^2)	(\AA^2)	(\AA^2)
154	66.5 ± 5.3	55.1 ± 0.6	1.66 ± 0.14
224	39.8 ± 2.5	47.1 ± 0.5	1.23 ± 0.08
293	33.0 ± 2.5	42.4 ± 0.4	1.06 ± 0.07

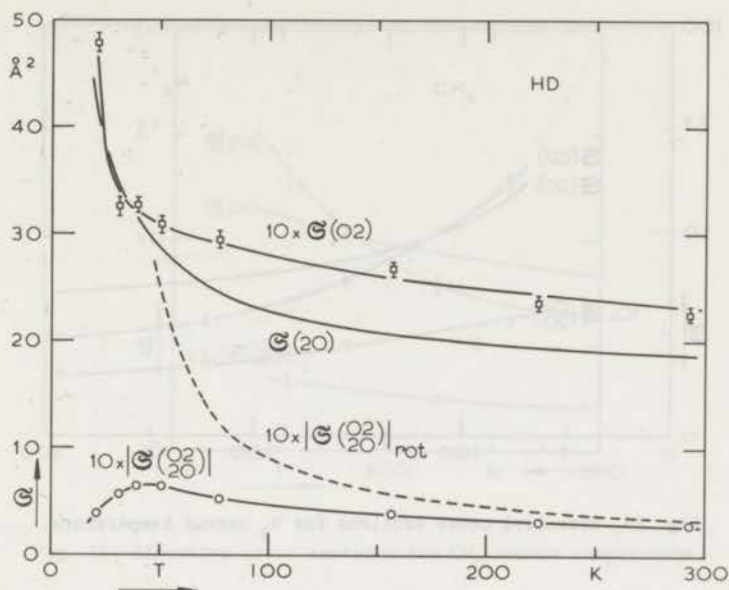


Fig. 12. Effective cross section for HD versus temperature. For the dotted line which represents $|\sigma_{20}^{(02)}|_{\text{rot}}$, see text.

$\sigma(02)$ with respect to $\sigma(20)$ it is found that HD collisions are rather ineffective in reorienting a molecule. The plot for $|\sigma_{20}^{(02)}|$ shows for HD a cross section which at first increases with decreasing temperature, and then below 45 K begins to decrease rapidly. This behaviour at the lower temperatures can be explained by the fact that molecules in the rotational state $J = 0$ do not contribute to the field effect. If HD in the $J = 0$ rotational state can be considered a "noble" gas as far as these experiments are concerned, then the expression for mixtures can be used (see ref. 24). This mixture is composed of rotating ($J \neq 0$) and non-rotating ($J = 0$) HD molecules, and the following expressions are obtained:

$$\Psi_{02} = x \frac{\{x \sigma_{20}^{(02)}_{\text{rot}} + (1-x) \sigma_{20}^{(02)}_{\text{rot-n.rot}}\}^2}{\{x \sigma_{20}^{(02)}_{\text{rot}} + (1-x) \sigma_{20}^{(02)}_{\text{rot-n.rot}}\} \sigma(20)} \quad (17)$$

and

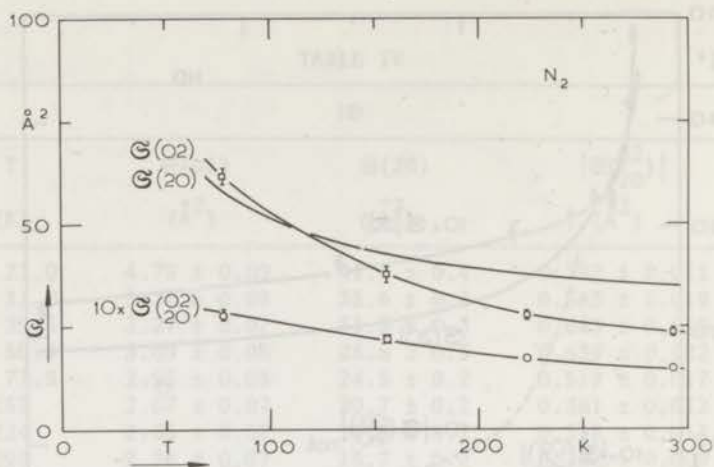


Fig. 13. Effective cross sections for N_2 versus temperature.

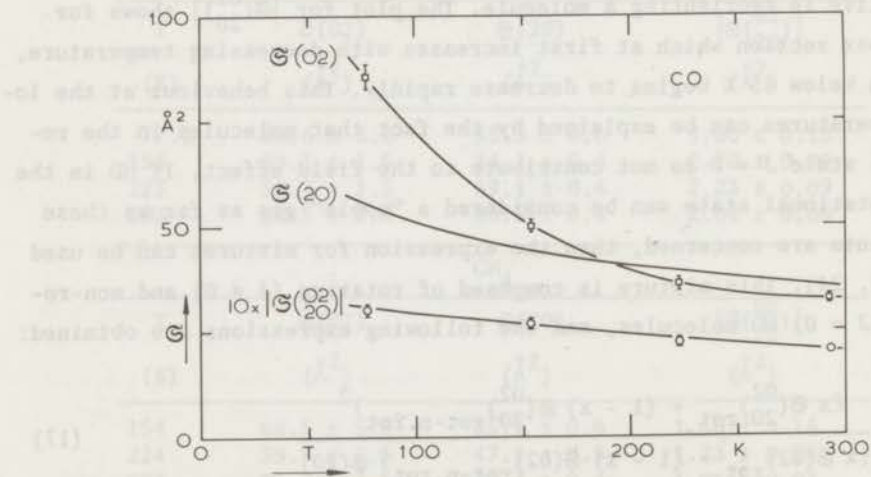


Fig. 14. Effective cross sections for CO versus temperature.

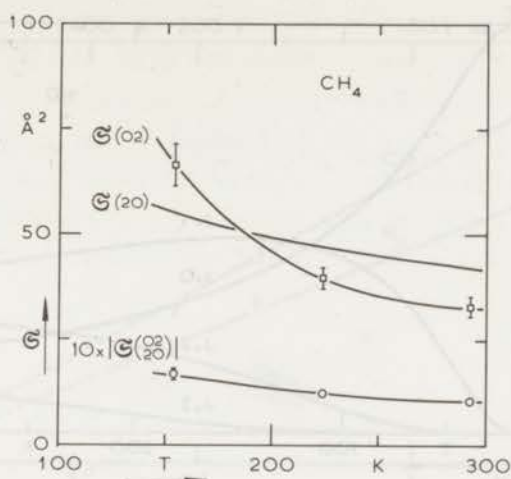


Fig. 15. Effective cross sections for CH_4 versus temperature.

$$\xi_{02} = \frac{1}{\langle v_{\text{rel}} \rangle_0 \{ x \sigma_{\text{rot}}^{(02)} + (1 - x) \sigma_{\text{rot-n.rot}}^{(02)} \}} \frac{g \mu_N kT}{\hbar} \frac{H}{P} \quad (18)$$

The quantity $\sigma_{\text{rot}}^{(02)}$ gives the production of $[J]^{(2)}$ polarization from the $[W]^{(2)}$ polarization while $\sigma_{\text{rot}}^{(02)}$ describes the reorientation of the $J \neq 0$ molecules. $\sigma_{\text{rot-n.rot}}^{(02)}$ and $\sigma_{\text{rot-n.rot}}^{(02)}$ give the production of $[J]^{(2)}$ polarization and the reorientation of the molecules in a gas in which the rotating molecules are infinitely diluted. The quantity x is the fraction of rotating molecules which can be calculated by $x = \sum_{J \neq 0} P_J$ where P_J is the fractional population of the J state given by:

$$P_J = \frac{(2J + 1) \exp \{-J(J + 1) \theta/T\}}{\sum_J (2J + 1) \exp \{-J(J + 1) \theta/T\}} \quad (19)$$

For HD ($\theta = 63.8$ K) the occupation of the different rotational levels as a function of the temperature is illustrated in fig. 16. Under certain

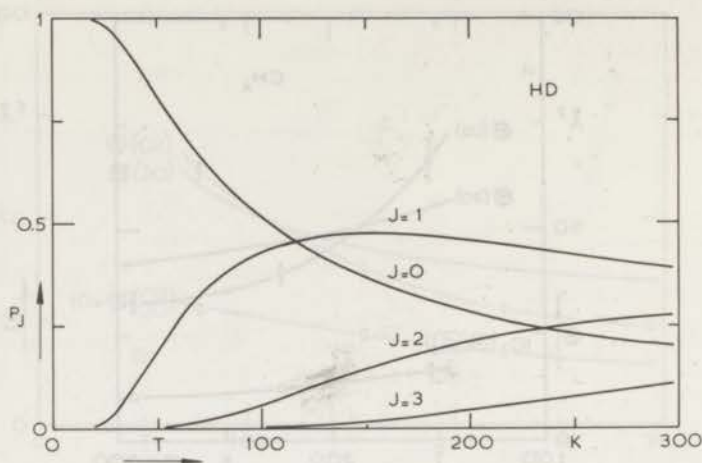


Fig. 16. The populations of different rotational levels for HD versus temperature.

assumptions with respect to $\mathfrak{S}_{(20)}^{(02)}_{\text{rot-n.rot}}$ the quantity $|\mathfrak{S}_{(20)}^{(02)}_{\text{rot}}|$ can be obtained as a function of temperature. In fig. 12 $|\mathfrak{S}_{(20)}^{(02)}_{\text{rot}}|$ is plotted for $\mathfrak{S}_{(20)}^{(02)}_{\text{rot-n.rot}} = \frac{1}{2} \mathfrak{S}_{(20)}^{(02)}_{\text{rot}}$. This assumption can be justified by the experiments done on mixtures with noble gases²⁴. It is seen that the dependence on temperature of $|\mathfrak{S}_{(20)}^{(02)}_{\text{rot}}|$ for HD does not essentially differ from that for $|\mathfrak{S}_{(20)}^{(02)}|$ of the gases N_2 , CO and CH_4 which have smaller rotational constants.

For the gases N_2 , CO and CH_4 the reorientation cross section $\mathfrak{S}(02)$ has a steep temperature dependence and becomes at lower temperatures even larger than the gas-kinetic cross section. Furthermore, the fact that the cross section $|\mathfrak{S}_{(20)}^{(02)}|$ is always much smaller than $\mathfrak{S}(02)$ means that the collisions are not very effective in producing a $[J]^{(2)}$ polarization from a $[W]^{(2)}$ polarization. Note that the field strength is always so high that the nuclear spin and the magnetic moment of the molecule are completely decoupled, so that the presence of the nuclear spin can be neglected in the magnetic field effects.

To get a better idea of the temperature dependence of the reorientation cross section of the gases N_2 and CO a plot is made of $\mathfrak{S}(02)$ versus T^{-1} , see fig. 17. It is seen that the temperature dependence in the investigated region can be described by:

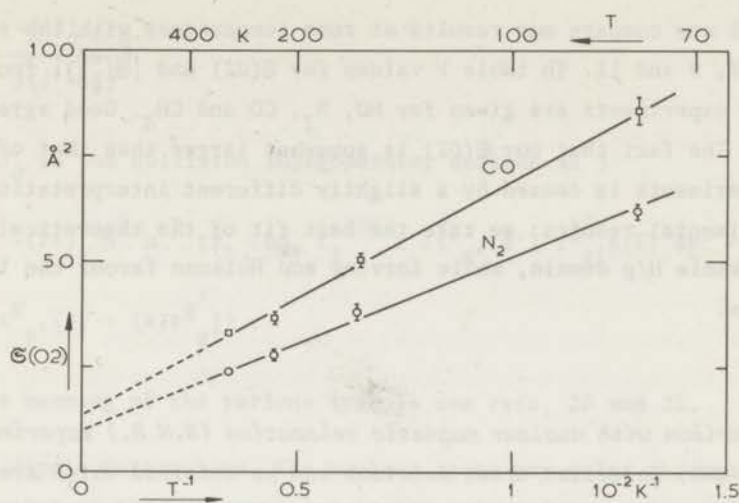


Fig. 17. The reorientation cross section for tensorial polarization $\mathfrak{E}(02)$ versus T^{-1} for N_2 and CO.

$$\mathfrak{E}(02) = a + bT^{-1} \quad (20)$$

with $a = 10 \text{ \AA}^2$ and $b = 41 \times 10^2 \text{ \AA}^2 \text{K}$ for N_2 while $a = 13.5 \text{ \AA}^2$ and $b = 55 \times 10^2 \text{ \AA}^2 \text{K}$ for CO.

TABLE V

Comparison with other data at room temperature

	$\mathfrak{E}(02)$ (\AA^2)			$ \mathfrak{E}_{20}^{(02)} $ (\AA^2)		
	this research	ref. 8	ref. 9	ref. 11	this research	ref. 9
HD	2.26 ± 0.07	2.3	2.2	-	0.282 ± 0.009	0.28
N_2	23.7 ± 0.9	22	22	21	1.49 ± 0.05	1.46
CO	32.5 ± 0.8	31	31	31	2.04 ± 0.06	1.97
CH_4	33.0 ± 2.5	32	30	32	1.06 ± 0.07	1.01

We will now compare our results at room temperature with the results of refs. 8, 9 and 11. In table V values for $\mathcal{E}(02)$ and $|\mathcal{E}_{20}^{(02)}|$ from the different experiments are given for HD, N₂, CO and CH₄. Good agreement is found. The fact that our $\mathcal{E}(02)$ is somewhat larger than that of the other experiments is caused by a slightly different interpretation of the experimental results: we take the best fit of the theoretical curves over the whole H/p domain, while Korving and Hulsman favour the lower H/p values.

5. A comparison with nuclear magnetic relaxation (N.M.R.) experiments.

Also from NMR, molecular cross sections can be obtained which are related to the reorientation of the molecules. Hence it is useful to compare $\mathcal{E}(02)$ obtained from our experiments with the NMR cross sections. First we will summarize the different mechanisms that can cause relaxation of the nuclear spin in diatomic molecules and in spherical top molecules. Only the extreme narrowing limit is considered.

5.1 Survey of relaxation mechanisms. Diatomic molecules.

In dilute gases of diatomic molecules three kinds of intramolecular relaxation can be distinguished.

Spin-rotation interaction. Nuclear spins may relax through an interaction with the rotational motion of the molecule which causes a local magnetic field at the site of a nucleus. Starting from the Waldmann-Snider equation Chen and Snider²⁵⁾ derived an expression for the relaxation times T_1 and T_2 in which the decay time is given explicitly in terms of a two particle collision integral. For a single rotational level with quantum number J it is found that

$$T_1^{-1} = T_2^{-1} = \frac{2}{3} c^2 J(J+1) \tau_1. \quad (21)$$

Here c is the spin-rotation coupling constant and τ_1 is the decay time for vectorial polarization of the rotational angular momentum J . It is given by:

$$\tau_1^{-1} = \frac{\langle \underline{J} \cdot R'_0 \underline{J} \rangle_0}{J(J+1)} \quad (22)$$

where R'_0 is the collision superoperator defined as*:

$$R'_0 \phi = -(2\pi)^4 \hbar^2 n^{-1} \text{tr}_1 \int d\underline{p}_1 f_1^{(0)} \{ \int t_{g',(\phi')}^g t_{g',\delta(E)}^{g+} dp' + \\ - \frac{i}{2\pi} [t_{g',(\phi)}^g - (\phi)t_{g'}^{g+}] \} \quad (23)$$

For the meaning of the various symbols see refs. 20 and 25.

Dipole-dipole interaction. The nuclear spins may relax through mutual interaction of the nuclear spins in the same molecule. For this intramolecular process Chen and Snider give expressions for the relaxation times of a single level system, which are given by:

$$T_1^{-1} = T_2^{-1} = \frac{2}{15} c_d^2 \frac{J(J+1)}{(2J-1)(2J+3)} (2I-1)(2I+3) a_1^2 \tau_2 \quad (24)$$

where I is the total spin of the molecule, a_1 is given by:

$$a_1 = \frac{I^2(I+1)^2 - 3[I_1(I_1+1) - I_2(I_2+1)]^2 + 2I(I+1)[I_1(I_1+1) + I_2(I_2+1)]}{2I(I+1)(2I-1)(2I+3)}$$

and $c_d = -6g_I^2 \mu_N^2 / 2 \hbar r^3$, where g_I is the nuclear g factor and r is the distance between the two nuclei which, in general, have different spins I_1 and I_2 . The decay time τ_2 for this mechanism is given in terms of collision integrals of the $[\underline{J}]^{(2)}$ rotational angular momentum:

$$\tau_2^{-1} = \frac{\langle [\underline{J}]^{(2)} : R'_0 [\underline{J}]^{(2)} \rangle_0}{\frac{1}{6} J(J+1)(2J-1)(2J+3)} \quad (25)$$

*The collision superoperator defined here differs from that given in eq. (16) in that the collision partner does not explicitly appear in R'_0 . This is a consequence of assuming that collisions cannot change nuclear spin states.

Quadrupole interaction. The nuclear spins may relax through interaction with the electric-field gradients of the molecule, if the nuclei possess a quadrupole moment. This occurs only for nuclei with spin greater than 1/2 and when present it is the dominant mechanism. This type of relaxation has not been discussed by Chen and Snider. Formally, however, the problem is quite analogous to the dipole-dipole situation. For quadrupole relaxation in diatomics two different cases have to be distinguished, *i.e.*, a. molecules in which only one of the nuclei is of importance for the relaxation and b. molecules in which both nuclei are identical and have spins greater than 1/2. For the molecules of type a., we find for a single level system:

$$T_1^{-1} = T_2^{-1} = \frac{3}{40} \frac{J(J+1)}{(2J-1)(2J+3)} \frac{2I_1+3}{I_1^2(2I_1-1)} \left(\frac{\text{eq}Q}{\hbar}\right)^2 \tau_2 \quad (26)$$

where τ_2 is the same quantity that occurs for the dipole-dipole relaxation given in eq. (25), I_1 is the spin quantum number of the relevant nucleus and $\text{eq}Q/\hbar$ the intramolecular quadrupole coupling constant. For molecules having two identical nuclei with a quadrupole moment it is found that (see also ref. 26):

$$T_1^{-1} = T_2^{-1} = \frac{3}{40} \frac{J(J+1)}{(2J-1)(2J+3)} \frac{(2I-1)(2I+3)}{I_1^2(2I_1-1)} \left\{ 1 - \frac{4I_1(I_1+1)+I(I+1)}{(2I-1)(2I+3)} \right\} \left(\frac{\text{eq}Q}{\hbar}\right)^2 \tau_2 \quad (27)$$

Multilevel system. To describe nuclear spin relaxation when many rotational levels are involved, some appropriate averaging must be introduced. By treating τ_1 and τ_2 as effective decay or correlation times, a simple Boltzmann averaging can be used, *viz.*

$$T_1^{-1} = T_2^{-1} = \frac{2}{3} c^2 \langle J(J+1) \rangle_0 \tau_1 \quad (28)$$

$$T_1^{-1} = T_2^{-1} = \frac{2}{15} c_d^2 \left\langle \frac{J(J+1)}{(2J-1)(2J+3)} (2I-1)(2I+3) a_1^2 \right\rangle_0 \tau_2 \quad (29)$$

$$T_1^{-1} = T_2^{-1} = \frac{3}{40} \left\langle \frac{J(J+1)}{(2J-1)(2J+3)} \frac{2I_1+3}{I_1^2(2I_1-1)} \right\rangle_0 \left(\frac{eqQ}{\hbar} \right)^2 \tau_2 \quad (30)$$

$$T_1^{-1} = T_2^{-1} = \frac{3}{40} \left\langle \frac{J(J+1)}{(2J-1)(2J+3)} \frac{(2I-1)(2I+3)}{I_1^2(2I_1-1)^2} \left\{ 1 - \frac{4I_1(I_1+1)+I(I+1)}{(2I-1)(2I+3)} \right\} \right\rangle_0 \left(\frac{eqQ}{\hbar} \right)^2 \tau_2 \quad (31)$$

for respectively spin-rotation, dipole-dipole and two cases of quadrupole relaxation in diatomic molecules (see also ref. 27). Note that for high J values eqs. (28) and (30) agree with the classical treatment of Gordon²⁸⁾, while eqs. (29) and (31) agree only for special values of I and I_1 .

Spherical top molecules. For spherical top molecules as CH_4 , CF_4 and CD_4 the relaxation mechanisms which are of importance are:

Spin-rotation interaction. This relaxation mechanism in spherical tops is treated by Dong and Bloom²⁹⁾ and McCourt and Hess³⁰⁾. The relaxation times are given by:

$$T_1^{-1} = T_2^{-1} = \frac{2}{3} \frac{\langle J(J+1) I(I+1) \rangle_0}{\langle I(I+1) \rangle_0} \left\{ c_a^2 + \frac{4}{45} c_d^2 \right\} \tau_1 \quad (32)$$

where I is the total spin, c_a and c_d are two independent coupling constants by which the spin-rotation interaction can be characterized. The quantity $\langle J(J+1)I(I+1) \rangle_0 / \langle I(I+1) \rangle_0$ can be calculated using the results of refs. 31 and 32. For temperatures which are not too low (> 100 K) it is equal to $3I_0 kT / \hbar^2$ where I_0 is the moment of inertia.

Quadrupole interaction. For this mechanism in spherical top molecules an expression is given by Bloom *et al.*³³⁾ using a correlation function approach which gives:

$$\tau_1^{-1} = \tau_2^{-1} = \frac{3}{8} \left(\frac{eqQ}{h} \right)^2 f_2 \tau_2 \quad (33)$$

with $f_2 = 0.2$ for spherical top molecules.

5.2 Comparison of cross sections. To compare the NMR data with our results we introduce also (effective) cross sections for NMR by:

$$\tau_i^{-1} = n \langle v_{rel} \rangle_0 \mathfrak{E}'(oi) \quad (34)$$

where $i = 1$ for spin-rotation and $i = 2$ for dipole-dipole and quadrupole relaxation. The prime refers to the collision superoperator which for NMR is different from that used in the viscosity cross sections, see eqs. (16) and (23). Thus the NMR cross sections are given by:

$$\mathfrak{E}'(01) = \frac{1}{\langle v_{rel} \rangle_0} \frac{\langle \underline{J} \cdot R'_0 \underline{J} \rangle_0}{\langle \underline{J} \cdot \underline{J} \rangle_0}; \quad \mathfrak{E}'(02) = \frac{1}{\langle v_{rel} \rangle_0} \frac{\langle [\underline{J}]^{(2)} : R'_0 [\underline{J}]^{(2)} \rangle_0}{\langle [\underline{J}]^{(2)} : [\underline{J}]^{(2)} \rangle_0} \quad (35)$$

Now we will treat successively the gases HD, N₂, CH₄, CF₄ and CD₄.

Hydrogen deuteride. It is possible to obtain from NMR experiments on HD both $\mathfrak{E}'(01)$ and $\mathfrak{E}'(02)$. In fig. 18 these quantities are calculated from the measurements done by Hardy³⁴ and compared with $\mathfrak{E}(02)$ from the field effect on viscosity. It can be seen that within the accuracy of both experiments $\mathfrak{E}(02)$ and $\mathfrak{E}'(02)$ are equal. From this result it can be concluded that the difference between R_0 and R'_0 is very small indicating that there is no direct transfer of $[\underline{J}]^{(2)}$ polarization during a collision. This supports one of the assumptions of a collisionally uncoupled model proposed by Coope and Snider for the contribution of orientational polarization to transport properties of dilute gases³⁵. $\mathfrak{E}'(01)$ is for lower temperatures close to $\mathfrak{E}'(02)$ while for higher temperatures it becomes smaller than $\mathfrak{E}'(02)$. The ratio $\mathfrak{E}'(02)/\mathfrak{E}'(01)$ varies from 1 to 1.35 in agreement with the appropriate limits ($1 < \tau_1/\tau_2 < 3$) given by Bloom and Oppenheim³³.

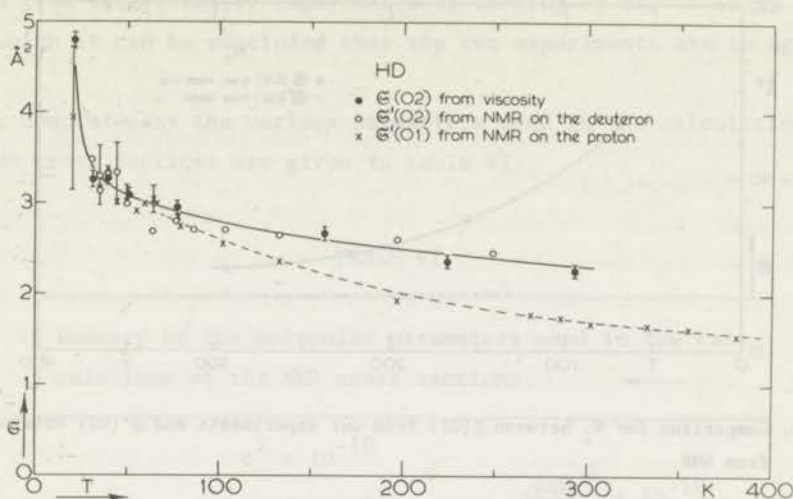


Fig. 18. Comparison for HD between $\epsilon(02)$ from our experiments and $\epsilon'(01)$ and $\epsilon'(02)$ obtained from NMR.

Nitrogen. NMR measurements on N_2 have been performed by Speight and Armstrong³⁶⁾ at rather high densities (100-600 amagat). The $\epsilon'(02)$ cross section calculated from these experiments using eqs. (31) and (34) is plotted in fig. (19) together with $\epsilon(02)$. A great discrepancy between both experiments is found. Since the densities are high in the NMR experiment, the gas may not be considered dilute, which may account for the disagreement. From this point of view NMR experiments for N_2 at lower densities are desirable.

Methane. For CH_4 the spin-rotation mechanism is dominant giving the $\epsilon'(01)$ cross section from NMR measurements. Using the data of ref. 33, this cross section is compared with our $\epsilon(02)$ in fig. 20. The ratio $\epsilon(02)/\epsilon'(01)$ is about 1.85 for all temperatures.

Tetrafluoromethane. For CF_4 field dependent viscosity measurements have been performed at room temperature by Korving¹¹⁾ and Hulsman *et al.*⁹⁾. With these results and those obtained from the NMR measurements of Dong and Bloom²⁹⁾ for $\epsilon'(01)$, we find that the ratio $\epsilon(02)/\epsilon'(01)$ is about 1.6.

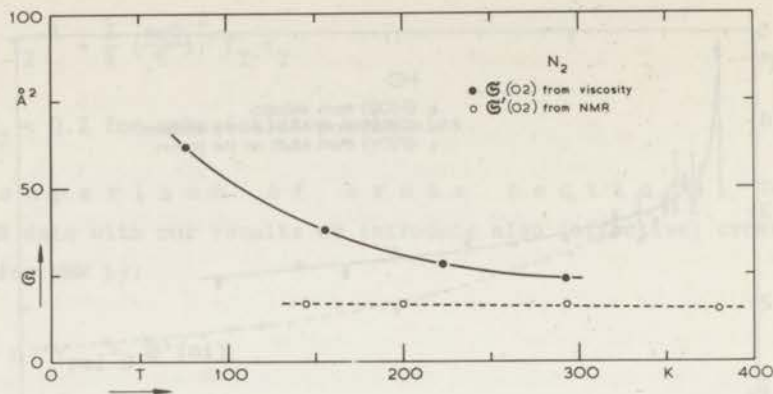


Fig. 19. Comparison for N_2 between $\sigma(O_2)$ from our experiments and $\sigma'(O_2)$ obtained from NMR.

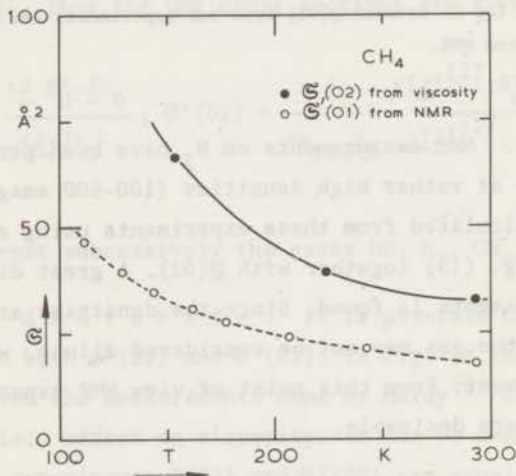


Fig. 20. Comparison for CH_4 between $\sigma(O_2)$ from our experiments and $\sigma'(O_1)$ obtained from NMR.

Tetraduteromethane. In CD_4 relaxation occurs through a quadrupole mechanism. The coupling constant eqQ/\hbar for this gas, however, is not known experimentally. Using estimated values as given in ref. 33 the $\sigma'(O_2)$ cross section at room temperature obeys the following inequality: $21 \text{ \AA}^2 \leq \sigma'(O_2) \leq 49 \text{ \AA}^2$. The value of $\sigma(O_2)$ ob-

tained from the viscosity experiments of Korving *et al.*¹⁰⁾ is 21 \AA^2 , from which it can be concluded that the two experiments are in agreement.

For completeness the various parameters used in the calculations of the NMR cross sections are given in table VI.

TABLE VI

Summary of the molecular parameters used in the calculations of the NMR cross sections.

	$c^2 \times 10^{-10}$	$\left(\frac{eqQ}{h}\right)^2 \times 10^{-10}$
	$(c_a^2 + \frac{4}{45} c_d^2) \times 10^{-10}$	
	($\text{rad}^2 \text{ sec}^{-2}$)	($\text{rad}^2 \text{ sec}^{-2}$)
HD	30.0	203
N ₂		121×10^3
CH ₄	0.54	
CF ₄	0.16	
CD ₄		66 - 159

Similar information on reorientation of molecules can be obtained from depolarized Rayleigh light scattering experiments. A comparison between results of these experiments and those discussed here will be given in ref. 37.

REFERENCES

1. Beenakker, J.J.M., Festkörperprobleme VIII, ed. O. Madelung, Vieweg Verlag (Braunschweig, 1968) p. 276.
2. Beenakker, J.J.M. and McCourt, F.R., Ann.Rev.Phys.Chem. 21 (1970) 47.
3. Hooyman, G.J., Mazur, P. and De Groot, S.R., Physica 21 (1955) 355.
4. De Groot, S.R. and Mazur, P., Non-equilibrium Thermodynamics, (North-Holland Publishing Comp., Amsterdam, 1962) p. 311.
5. Coope, J.A.R. and Snider, R.F., J.Chem.Phys. 56 (1972) 2056.
6. Hess, S. and Waldmann, L., Z. Naturforsch. 26a (1971) 1057.
7. Hulsman, H. and Burgmans, A.L.J., Phys. Letters 29A (1969) 629.
8. Hulsman, H., van Waasdijk, E.J., Burgmans, A.L.J., Knaap, H.F.P. and Beenakker, J.J.M., Physica 50 (1970) 53 (Commun. Kamerlingh Onnes Lab., Leiden No. 381c).
9. Hulsman, H., van Kuik, F.G., Walstra, K.W., Knaap, H.F.P. and Beenakker, J.J.M., Physica 57 (1972) 501 (Commun. Kamerlingh Onnes Lab., Leiden No. 389e).
10. Korving, J., Hulsman, H., Scoles, G., Knaap, H.F.P. and Beenakker, J.J.M., Physica 36 (1967) 177 (Commun. Kamerlingh Onnes Lab., Leiden No. 357b).
11. Korving, J., Physica 50 (1970) 27 (Commun. Kamerlingh Onnes Lab., Leiden No. 381b).
12. Van Ee, H., Thesis Leiden (1966) p. 21.
13. Hulsman, H., and Knaap, H.F.P., Physica 50 (1970) 565 (Commun. Kamerlingh Onnes Lab., Leiden No. 383b).
14. Hirschfelder, J.O., Curtiss, C.F. and Bird, R.B., Molecular theory of gases and liquids, (John Wiley and Sons, Inc. New York, 1954) p. 545.
15. Kohlrausch, F., Praktische Physik, (B.G. Teubner Verlagsgesellschaft, Stuttgart, 1968) Band I, p. 178.
16. Loeb, L.B., The kinetic theory of gases, (McGraw Hill Book Cy., Inc. New York and London, 1934) p. 297.
17. Moraal, H., McCourt, F.R. and Knaap, H.F.P., Physica 45 (1969) 455. (Commun. Kamerlingh Onnes Lab., Leiden, Suppl. No. 127d).

18. Prangmsma, G.J., Thesis Leiden (1971) p. 60.
Prangmsma, G.J., Burgmans, A.L.J., Knaap, H.F.P. and Beenakker, J.J.M.,
Physica, to be published.
19. McCourt, F.R. and Moraal, H., Chem.Phys.Letters 9 (1971) 39.
20. Levi, A.C., McCourt, F.R. and Tip, A., Physica 39 (1968) 165 (Com-
mun. Kamerlingh Onnes Lab., Leiden, Suppl. No. 126b).
21. Data Book, edited by Thermophysical Properties Research Center,
Purdue University (Lafayette, Indiana, 1966) Vol. 2.
22. Rietveld, A.O., van Itterbeek, A. and Velds, C.A., Physica 25
(1959) 205 (Commun. Kamerlingh Onnes Lab., Leiden No. 314b).
23. Baas, F., Phys. Letters 36A (1971) 107.
24. This thesis, chapter II.
Burgmans, A.L.J. *et al.*, Physica, to be published.
25. Chen, F.M. and Snider, R.F., J.Chem.Phys. 48 (1968) 3185.
26. Ramsey, N.F., Molecular Beams, (Oxford University Press, 1963)
p. 214.
27. Bloom, M. and Oppenheim, I., Canad.J.Phys. 41 (1963) 1580.
28. Gordon, R.G., J.Chem.Phys. 44 (1966) 228.
29. Dong, R.Y. and Bloom, M., Canad.J.Phys. 48 (1970) 793.
30. McCourt, F.R. and Hess, S., Z. Naturforsch. 26a (1971) 1234.
31. Yi, P., Ozier, I. and Anderson, C.H., Phys.Rev. 165 (1968) 92.
32. Bright Wilson, Jr., E., J.Chem.Phys. 3 (1935) 276.
33. Bloom, M., Bridges, F. and Hardy, W.N., Canad.J.Phys. 45 (1967)
3533.
34. Hardy, W.N., Thesis Vancouver (1964) p. 96.
35. Coope, J.A.R. and Snider, R.F., J.Chem.Phys. 56 (1972) 2049.
36. Speight, P.A. and Armstrong, R.L., Canad.J.Phys. 47 (1969) 1475.
37. Keijser, R.A.J. *et al.*, to be published.

CHAPTER II

THE CONCENTRATION DEPENDENCE
OF THE VISCOMAGNETIC EFFECT

1. *Introduction.* In chapter I¹⁾ experiments have been reported on the temperature dependence of the magnetic field effect on viscosity in pure gases consisting of non-spherical molecules. In this chapter we will present results obtained from similar experiments on mixtures of polyatomic gases with noble gases.

The shear viscosity of a gas of polyatomic molecules in a magnetic field can be described by five independent coefficients, *i.e.*, according to the notation of Coope and Snider²⁾: η_0^+ , η_1^+ , η_2^+ , η_1^- and η_2^- (see also ref. 3). Theoretical expressions for these coefficients can be obtained from a Chapman-Enskog treatment of the field effect⁴⁾, in which the non-equilibrium distribution function is expanded in terms of irreducible tensors made up of reduced velocity \underline{W} and angular momentum \underline{J} . From the experiments it is seen that in simple gases⁵⁻⁷⁾ and in mixtures of these gases with noble gases⁸⁾ the field effect on viscosity is dominated by one type of angular momentum polarization only, *viz.* $[\underline{J}]^{(2)}$. Hence the experimental results can be characterized by two parameters, one for the magnitude of the viscosity change and one for the field strength at which the effect occurs. These quantities are related to collision integrals, which are determined mainly by the anisotropic interaction between molecules. Consequently these experiments provide direct information about the non-spherical part of the molecular interaction.

Because the interaction between non-spherical and spherical particles is simpler to describe than the interaction between two non-spherical particles we have extended our investigations to mixtures of polyatomic gases (non-spherical) with noble gases (spherical). In order to test non-spherical potentials which describe such interactions, one needs

information on the collision integrals over a large temperature range. For this reason experiments have been performed as a function of temperature.

The systems HD-He, HD-Ne, HD-Ar, N₂-He, N₂-Ne and N₂-Ar have been investigated both at 77 K and 293 K. The field effect for each system has been studied as a function of the noble gas fraction by performing experiments at various compositions.

2. *Theory.* On pure gases extensive theoretical work has been done concerning the magnetic field effects on transport properties. For a survey see ref. 9. For mixtures consisting of linear diatomic molecules, a classical treatment of the shear viscosity tensor is given by Tip¹⁰. More recently a formal theory for mixtures was given by Raum and Köhler¹¹, based on the Waldmann-Snyder kinetic equation. In the calculations of ref. 10 the contribution of the dominant [J]⁽²⁾ polarization has been considered. Explicit expressions are given for the viscosity coefficients of binary mixtures in which one of the components is a noble gas. For such systems the field effect is found to be the same as for pure gases, and for the coefficients measured in our experimental situation, the functional form is given by:

$$\frac{\eta_1^+ + \eta_2^+ - 2\eta(0)}{2\eta(0)} = -\frac{1}{2} \psi_{02} \left[\frac{\xi_{02}^2}{1 + \xi_{02}} + \frac{4\xi_{02}^2}{1 + 4\xi_{02}} \right], \quad (1)$$

where $\eta(0)$ is the field free viscosity of the gas mixture. The expressions for ξ_{02} and ψ_{02} are, however, more complicated than for pure gases. The shape of the curve given by this expression as a function of ξ_{02} (or H/p) has a dispersion-like character reaching saturation for high values of ξ_{02} .

2.1 Position of the effect on the H/p axis. The quantity ξ_{02} fixes the position of the effect on the H/p axis and is determined by the decay of the tensorial polarization, [J]_A⁽²⁾. The subscript A is used here to denote the molecular species upon which experiments are performed. In pure polyatomic gases the decay

of this polarization is a consequence of collisions between identical molecules and can be expressed by the reorientation cross section for tensorial polarization, $\Xi(02)_A$. The subscript A now refers to the interactions* which are taking place in a pure gas consisting only of molecules A. In mixtures with a noble gas (component B) the decay of $[J_A]^{(2)}$ polarization may result from two kinds of interactions: collisions of the type A-A and of the type A-B. The decay through the interaction A-B is expressed by a cross section, denoted as $\Xi(02A)_{AB}$. The A between the brackets refers to the polarization of the polyatomic molecule considered, while the subscript AB refers to the interaction. For the proper definition of $\Xi(02A)_{AB}$ see table I, in which the cross sections are defined (see *e.g.* refs. 1 and 13). The expression for ξ_{02} can be written¹⁰⁾ in terms of the cross sections $\Xi(02)_A$ and $\Xi(02A)_{AB}$:

$$\xi_{02} = \{x_A \langle v_A \rangle_0 \Xi(02)_A + x_B \langle v_{AB} \rangle_0 \Xi(02A)_{AB}\}^{-1} \frac{g \mu_N kT}{\hbar} \frac{H}{P}, \quad (2)$$

where x_A and x_B are the mole fractions of the two components ($x_A + x_B = 1$). The mean relative velocities are given by:

$$\langle v_A \rangle_0 = \left(\frac{8kT}{\pi \mu_A}\right)^{1/2} \quad \text{and} \quad \langle v_{AB} \rangle_0 = \left(\frac{8kT}{\pi \mu_{AB}}\right)^{1/2} \quad (3)$$

with μ_A and μ_{AB} the reduced masses which are $m_A/2$ and $m_A m_B / (m_A + m_B)$, respectively. The quantity g is the molecular g-factor and μ_N the nuclear magneton. The other symbols have their usual meaning. From the experiments one determines the $(H/p)_{1/2}$ value, that is the value of H/p for which the effect reaches half saturation. This is given by [see also eq. (1)]:

$$\frac{(H/p)_{1/2}}{2} = \left(\frac{2^{1/2} g \mu_N kT}{\hbar}\right)^{-1} \{x_A \langle v_A \rangle_0 \Xi(02)_A + x_B \langle v_{AB} \rangle_0 \Xi(02A)_{AB}\}. \quad (4)$$

* In discussions for which only pure gases are considered the subscript A is dropped (see *e.g.* ref. 12 and the appendix of ref. 7).

TABLE I

Definition of the cross sections used in this paper

for pure polyatomic gases (A)

$$\begin{aligned} \mathfrak{S}_{(20)A} &= \frac{1}{\langle v_A \rangle_0} \frac{\langle [W_A]^{(2)} : R_0 [W_A]^{(2)} \rangle_0}{\langle [W_A]^{(2)} : [W_A]^{(2)} \rangle_0}; \quad \mathfrak{S}_{(02)A} = \frac{1}{\langle v_A \rangle_0} \frac{\langle [J_A]^{(2)} : R_0 [J_A]^{(2)} \rangle_0}{\langle [J_A]^{(2)} : [J_A]^{(2)} \rangle_0} \\ \mathfrak{S}_{(20)A}^{(02)} &= \frac{1}{\langle v_A \rangle_0} \frac{\langle [J_A]^{(2)} : R_0 [W_A]^{(2)} \rangle_0}{\langle [J_A]^{(2)} : [J_A]^{(2)} \rangle_0^{1/2} \langle [W_A]^{(2)} : [W_A]^{(2)} \rangle_0^{1/2}} \end{aligned}$$

where

$$\begin{aligned} R_0 \phi &= -(2\pi)^4 \pi^2 n^{-1} \text{tr}_1 \int dp_1 f_1^{(0)} \{ t_{g'}^g(\phi' + \phi_1') t_{g'}^{g+} \delta(E) dp' + \\ &- \frac{i}{2\pi} [t_{g'}^g(\phi + \phi_1) - (\phi + \phi_1) t_{g'}^{g+}] \}, \text{ see ref. 14.} \end{aligned}$$

for mixtures of a polyatomic gas (A) and a noble gas (B)

$$\begin{aligned} \mathfrak{S}_{(20A)AB} &= \frac{1}{\langle v_{AB} \rangle_0} \frac{\langle [W_A]^{(2)} : R_0^{AB} [W_A]^{(2)} \rangle_0}{\langle [W_A]^{(2)} : [W_A]^{(2)} \rangle_0}; \\ \mathfrak{S}_{(20B)AB} &= \frac{1}{\langle v_{AB} \rangle_0} \frac{\langle [W_B]^{(2)} : R_0^{AB} [W_B]^{(2)} \rangle_0}{\langle [W_B]^{(2)} : [W_B]^{(2)} \rangle_0} \\ \mathfrak{S}_{(20B)AB}^{(20A)} &= \frac{1}{\langle v_{AB} \rangle_0} \frac{\langle [W_A]^{(2)} : R_0^{AB} [W_B]^{(2)} \rangle_0}{\langle [W_A]^{(2)} : [W_A]^{(2)} \rangle_0^{1/2} \langle [W_B]^{(2)} : [W_B]^{(2)} \rangle_0^{1/2}} \\ \mathfrak{S}_{(02A)AB} &= \frac{1}{\langle v_{AB} \rangle_0} \frac{\langle [J_A]^{(2)} : R_0^{AB} [J_A]^{(2)} \rangle_0}{\langle [J_A]^{(2)} : [J_A]^{(2)} \rangle_0} \\ \mathfrak{S}_{(20A)AB}^{(02A)} &= \frac{1}{\langle v_{AB} \rangle_0} \frac{\langle [J_A]^{(2)} : R_0^{AB} [W_A]^{(2)} \rangle_0}{\langle [J_A]^{(2)} : [J_A]^{(2)} \rangle_0^{1/2} \langle [W_A]^{(2)} : [W_A]^{(2)} \rangle_0^{1/2}} \\ \mathfrak{S}_{(20B)AB}^{(02A)} &= \frac{1}{\langle v_{AB} \rangle_0} \frac{\langle [J_A]^{(2)} : R_0^{AB} [W_B]^{(2)} \rangle_0}{\langle [J_A]^{(2)} : [J_A]^{(2)} \rangle_0^{1/2} \langle [W_B]^{(2)} : [W_B]^{(2)} \rangle_0^{1/2}} \end{aligned}$$

where

$$\begin{aligned} R_0^{AB} \phi &= -(2\pi)^4 \pi^2 n_B^{-1} \text{tr}_B \int dp_B f_B^{(0)} \{ t_{g'_{AB}}^{g_{AB}}(\phi') t_{g'_{AB}}^{g_{AB}+} \delta(E) dp'_B + \\ &- \frac{i}{2\pi} [t_{g'_{AB}}^{g_{AB}}(\phi) - (\phi) t_{g'_{AB}}^{g_{AB}+}] \}, \text{ see also ref. 11.} \end{aligned}$$

Thus theory predicts a linear behaviour of the $(H/p)_{1/2}$ values *versus* the noble gas mole fraction x_B .

2.2 The magnitude of the field effect .

The magnitude of the field effect on viscosity, described by Ψ_{02} , is mainly determined by the strength of the coupling between the anisotropies in the angular momentum space and in the velocity space. In pure gases this coupling is characterized by the cross section $\mathfrak{S}_{(20)_A}^{(02)_A}$ which describes the production of $[\underline{J}_A]^{(2)}$ polarization from a $[\underline{W}_A]^{(2)}$ polarization through the interaction of the type A-A (see also earlier footnote). The quantity Ψ_{02} is in this case given by:

$$\Psi_{02} = \frac{\mathfrak{S}_{(20)_A}^{(02)_A}{}^2}{\mathfrak{S}_{(02)_A} \mathfrak{S}_{(20)_A}} \quad (\text{pure gases}), \quad (5)$$

where $\mathfrak{S}_{(20)_A}$ is the gas-kinetic cross section which can be obtained from the field free viscosity $\eta_A(0)$. In binary mixtures of polyatomic gases (A) with noble gases (B) the quantity Ψ_{02} is much more complicated. Now a tensor polarization $[\underline{J}_A]^{(2)}$ can be produced in different ways, *viz.*: a. from a $[\underline{W}_A]^{(2)}$ polarization through collisions of the type A-A, b. from a $[\underline{W}_A]^{(2)}$ polarization through collisions A-B and c. from a $[\underline{W}_B]^{(2)}$ polarization through collisions A-B. These three production mechanisms of $[\underline{J}_A]^{(2)}$ polarization can be described respectively by the cross sections $\mathfrak{S}_{(20)_A}^{(02)_A}$, $\mathfrak{S}_{(20A)_{AB}}^{(02A)_A}$ and $\mathfrak{S}_{(20B)_{AB}}^{(02A)_A}$. The last two cross sections are not independent, as can be readily seen by performing the average over the center of mass velocities. This results in the relation

$$\mathfrak{S}_{(20B)_{AB}}^{(02A)_A} = \frac{m_A}{m_B} \mathfrak{S}_{(20A)_{AB}}^{(02A)_A}, \quad (6)$$

where m_A and m_B are the masses of the molecules. Hence the magnitude of the field effect is essentially determined by two cross sections which couple the polarization in velocity space to the polarization in the

angular momentum space. The expression for ψ_{02} is given in ref. 10 and can be written in terms of these cross sections

$$\psi_{02} = x_A \frac{\{x_A \langle v_{A>0}^{20} \mathcal{E}_{(20)A}^{(02)} + x_B \langle v_{AB>0} [B_A^{20} + (m_A/m_B) B_B^{20}] \mathcal{E}_{(20A)AB}^{(02A)}\}^2}{2 \{x_A \langle v_{A>0} \mathcal{E}_{(02)A} + x_B \langle v_{AB>0} \mathcal{E}_{(02A)AB}^{(02A)}\} \{x_A B_A^{20} + x_B B_B^{20}\}}. \quad (7)$$

Here B_A^{20} and B_B^{20} are functions of gas-kinetic cross sections which determine the field free viscosity of the mixture, and are given by:

$$B_A^{20} = \frac{25}{2} x_A x_B \{x_B \langle v_{B>0} \mathcal{E}_{(20)B} + \langle v_{AB>0} [x_A \mathcal{E}_{(20B)AB}^{(20B)} - x_B \mathcal{E}_{(20B)AB}^{(20A)}]\} / d$$

and

$$B_B^{20} = \frac{25}{2} x_A x_B \{x_A \langle v_{A>0} \mathcal{E}_{(20)A} + \langle v_{AB>0} [x_B \mathcal{E}_{(20A)AB}^{(20A)} - x_A \mathcal{E}_{(20B)AB}^{(20A)}]\} / d, \quad (8)$$

where

$$d = \frac{25}{4} x_A x_B \{x_A \langle v_{A>0} \mathcal{E}_{(20)A} + x_B \langle v_{AB>0} \mathcal{E}_{(20A)AB}^{(20A)}\} x \{x_B \langle v_{B>0} \mathcal{E}_{(20)B} + x_A \langle v_{AB>0} \mathcal{E}_{(20B)AB}^{(20B)}\} - \frac{25}{4} x_A^2 x_B^2 \langle v_{AB>0}^2 \mathcal{E}_{(20B)AB}^{(20A)2}.$$

Note that if only component A is present, eqs. (2) and (7) reduce to the expressions which describe the field effect in pure gases.

3. *Experiment.* To measure the magnetic field effect on the viscosity in mixtures we use apparatus I described in ref. 1. In principle the ap-

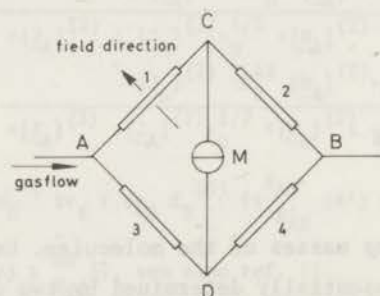


Fig. 1. Schematic diagram of the capillary bridge.

paratus is a Wheatstone bridge for gasflow, see fig. 1, in which one of the circular capillaries is placed between the poles of a magnet (Oerlikon C 3) perpendicular to the field direction. Starting from a steady state situation the magnetic field is switched on, causing a change in the viscosity in capillary 1. Consequently a pressure difference $p_C - p_D$ appears which is measured with the differential capacitance manometer (M) having a sensitivity of better than 10^{-5} torr (Varian MMM). This pressure difference is related to a combination of viscosity coefficients¹⁵⁾ which can be calculated from:

$$-\frac{\eta_1^+ + \eta_2^+ - 2\eta(0)}{2\eta(0)} = 4 \frac{p_C - p_D}{p_A - p_B} f, \quad (9)$$

where f a correction factor of the order unity given by:

$$f = \frac{2(p_C + K_\alpha)}{(p_A + K_\alpha) + (p_B + K_\alpha)} \left[1 + \frac{1}{16} \frac{R}{l} \operatorname{Re} \left(1 + \ln \frac{p_A}{p_C} \right) \right] \left(1 + \frac{K_\beta}{p} \right). \quad (10)$$

This factor has been discussed in detail in ref. 1 and is constructed from three different parts:

a. $2(p_C + K_\alpha) / [(p_A + K_\alpha) + (p_B + K_\alpha)]$ which corrects for the expansion of the gas and Knudsen effects on the field free flow, and usually has a value of about 1.3. The quantity K_α is calculated from $K_\alpha = n_\alpha p \xi / R$, where $p = \frac{1}{2}(p_A + p_C)$ and R the radius of the capillary. For n_α the value 4 is used in accordance with ref. 16 while ξ is the mean free path of the molecules given by $x_A \xi_A + x_B \xi_B$, where ξ_A and ξ_B are the mean free paths of molecules A and B. For a binary mixture they are given by Chapman and Cowling¹⁷⁾:

$$\xi_A^{-1} = 2^{1/2} \pi n_A \sigma_A^2 + \pi n_B \sigma_{AB}^2 (1 + m_A/m_B)^{1/2}$$

and

$$\xi_B^{-1} = 2^{1/2} \pi n_B \sigma_B^2 + \pi n_A \sigma_{AB}^2 (1 + m_B/m_A)^{1/2} \quad (11)$$

where n_A and n_B are the number densities and σ_{AB} is the average value of the molecular diameters σ_A and σ_B .

b. $[1 + (1/16) (R/Z) \text{Re} \{1 + \ln(p_A/p_C)\}]$ takes into account additional pressure losses at the entrance of the capillary and also in the capillary. The correction is usually small, having a value between 1 and 1.01. The quantity l is the length of the capillary, and Re is Reynolds number.

c. $1 + K_B/p$ corrects for Knudsen effects in the magnitude of the field effect.

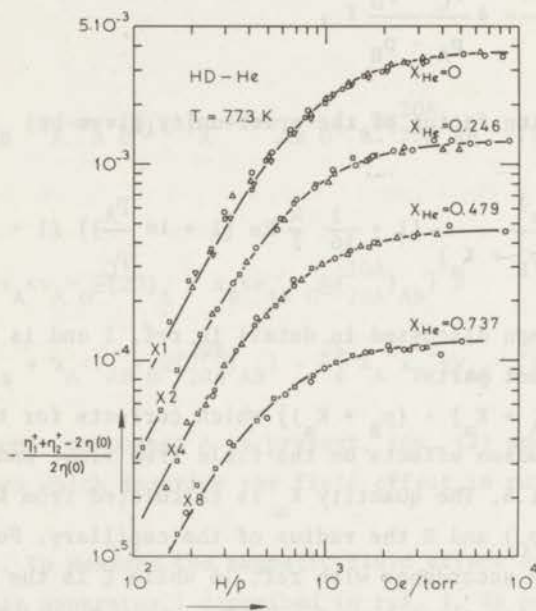


Fig. 2. $-[\eta_1^+ + \eta_2^+ - 2\eta(0)]/2\eta(0)$ versus H/p for various compositions of the system HD-He at 77.3 K.

To distinguish the four different curves for $x_{\text{He}} = 0; 0.246; 0.479$ and 0.737 , they are vertically shifted by dividing them respectively by 1, 2, 4 and 8.

$x_{\text{He}} = 0$: \circ 3.48 torr; Δ 4.65 torr; ∇ 9.45 torr; \square 15.7 torr.

$x_{\text{He}} = 0.246$: \circ 2.50 torr; Δ 7.66 torr; \square 17.9 torr.

$x_{\text{He}} = 0.479$: \circ 3.31 torr; Δ 8.16 torr; \square 18.6 torr.

$x_{\text{He}} = 0.737$: \circ 4.65 torr; \square 9.03 torr.

— theoretical H/p dependence, scaled to the experimental points.

The H/p values are also affected by Knudsen effects⁶⁾ and the correction is given by:

$$\frac{H}{P} = \frac{(H/p)_{\text{exp}}}{1 + K_V/p} \quad (12)$$

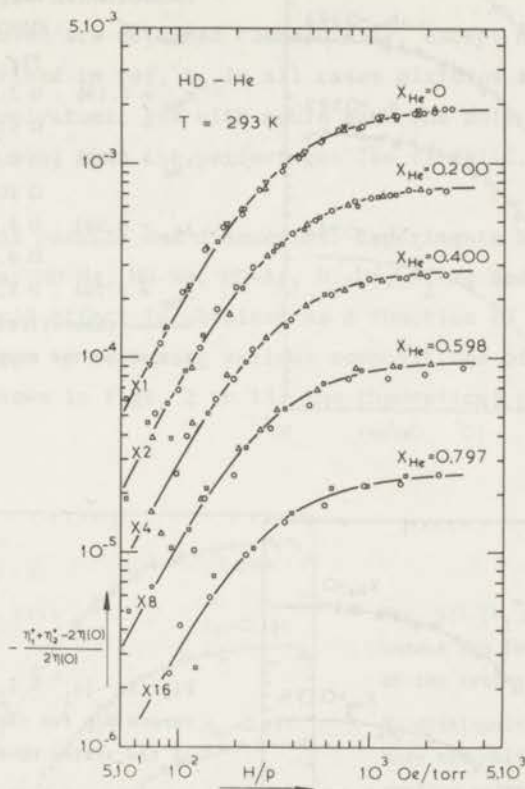


Fig. 3. $-\frac{[\eta_1^+ + \eta_2^+ - 2\eta(0)]}{2\eta(0)}$ versus H/p for various compositions of the system HD-He at 293 K.

To distinguish the different curves, they are shifted in the vertical direction as in fig. 2.

$x_{\text{He}} = 0$: 0 9.76 torr; Δ 12.4 torr; ∇ 15.6 torr; \square 20.8 torr.

$x_{\text{He}} = 0.200$: 0 10.6 torr; Δ 15.1 torr; \square 21.1 torr.

$x_{\text{He}} = 0.400$: 0 10.8 torr; Δ 15.3 torr; \square 20.1 torr.

$x_{\text{He}} = 0.598$: 0 8.28 torr; Δ 13.1 torr; \square 20.1 torr.

$x_{\text{He}} = 0.797$: 0 11.9 torr; \square 18.3 torr.

— theoretical H/p dependence, scaled to the experimental points.

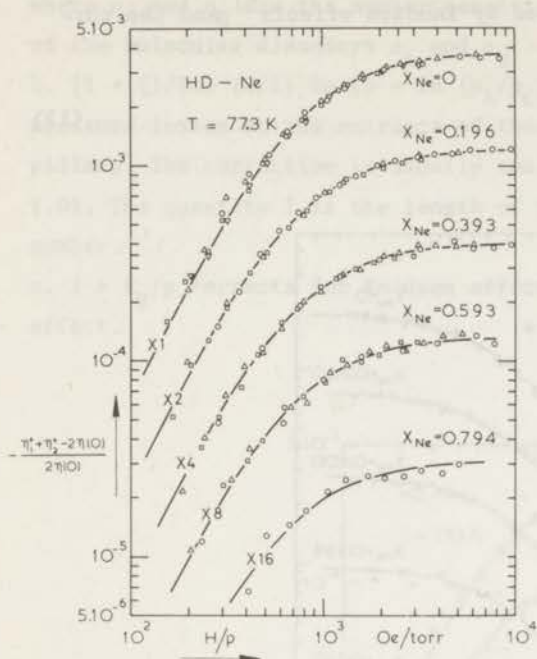


Fig. 4. $-\left[\eta_1^+ + \eta_2^+ - 2\eta(0)\right]/2\eta(0)$ versus H/p for various compositions of the system HD-Ne at 77.3 K.

To distinguish the different curves, they are shifted in the vertical direction as in fig. 2.

$x_{\text{Ne}} = 0$: $\circ\Delta\nabla\square$ points taken from fig. 2.

$x_{\text{Ne}} = 0.196$: \circ 2.99 torr; Δ 5.89 torr;
 \square 9.28 torr.

$x_{\text{Ne}} = 0.393$: \circ 2.93 torr; Δ 4.94 torr;
 \square 10.3 torr.

$x_{\text{Ne}} = 0.593$: \circ 3.68 torr; Δ 5.63 torr;
 \square 9.80 torr.

$x_{\text{Ne}} = 0.794$: \circ 5.74 torr.

— theoretical H/p dependence, scaled to the experimental points.

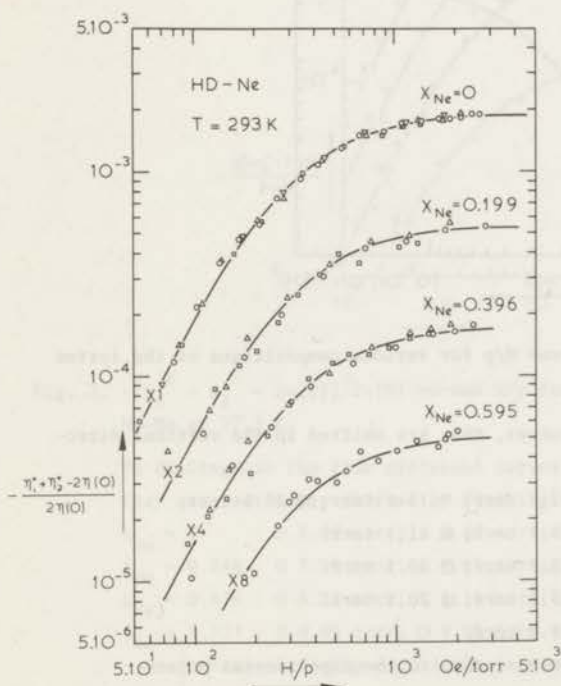


Fig. 5. $-\left[\eta_1^+ + \eta_2^+ - 2\eta(0)\right]/2\eta(0)$ versus H/p for various compositions of the system HD-Ne at 293 K.

To distinguish the different curves, they are shifted in the vertical direction as in fig. 2.

$x_{\text{Ne}} = 0$: $\circ\Delta\nabla\square$ points taken from fig. 3.

$x_{\text{Ne}} = 0.199$: \circ 9.12 torr; Δ 14.7 torr;
 \square 21.9 torr.

$x_{\text{Ne}} = 0.396$: \circ 10.7 torr; Δ 14.8 torr;
 \square 19.3 torr.

$x_{\text{Ne}} = 0.595$: \circ 13.6 torr.

— theoretical H/p dependence, scaled to the experimental points.

The quantities K_β and K_γ are determined experimentally by extrapolating to infinite pressure. Analogous to K_α , these quantities can be written as $K_{\beta,\gamma} = n_{\beta,\gamma} p \xi_A/R$. For the mixtures investigated, the numbers n_β and n_γ are found to be the same as for the pure gases¹⁾, i.e., $n_\beta = 10$ and $n_\gamma = 14$ for the HD-noble gas mixtures and $n_\beta = 10$ and $n_\gamma = 3$ for the N_2 -noble gas mixtures.

The gases used are obtained commercially, except HD which is prepared as described in ref. 1. In all cases mixtures are made by simply diluting the polyatomic gas with noble gas. The mole fractions are obtained by assuming that the perfect gas law is valid.

4. *Experimental results and discussion.* Experiments have been performed on the systems: HD-He, HD-Ne, HD-Ar, N_2 -He, N_2 -Ne and N_2 -Ar at 77 K and 293 K. The field effect is obtained as a function of the mole fraction of the noble gas by measuring various compositions of each system. The results are shown in figs. 2 to 13. The theoretical curves are given by

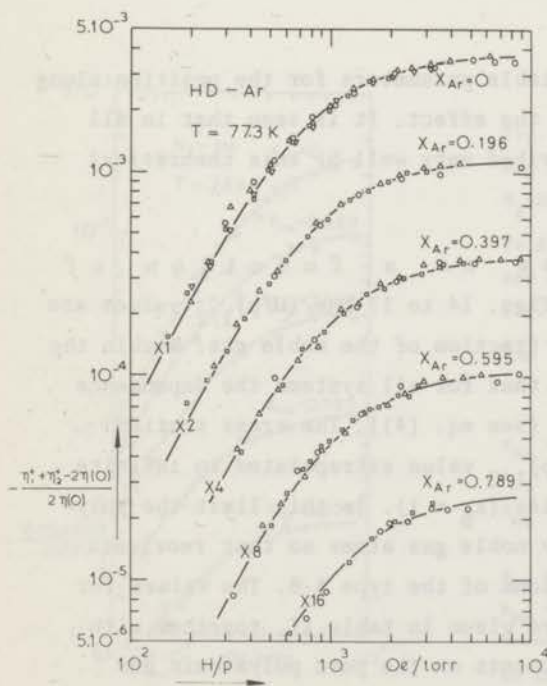


Fig. 6: $-\frac{[\eta_1^+ + \eta_2^+ - 2\eta(0)]}{2\eta(0)}$ versus H/p for various compositions of the system HD-Ar at 77.3 K.

To distinguish the different curves, they are shifted in the vertical direction as in fig. 2.

- $x_{Ar} = 0$: $\circ \Delta \nabla \square$ points taken from fig. 2.
 $x_{Ar} = 0.196$: \circ 1.45 torr; Δ 3.26 torr;
 \square 7.92 torr.
 $x_{Ar} = 0.397$: \circ 2.65 torr; Δ 3.25 torr;
 \square 6.54 torr.
 $x_{Ar} = 0.595$: \circ 2.56 torr; Δ 5.12 torr;
 \square 7.71 torr.
 $x_{Ar} = 0.789$: \circ 2.94 torr; \square 4.61 torr.
 — theoretical H/p dependence, scaled to the experimental points.

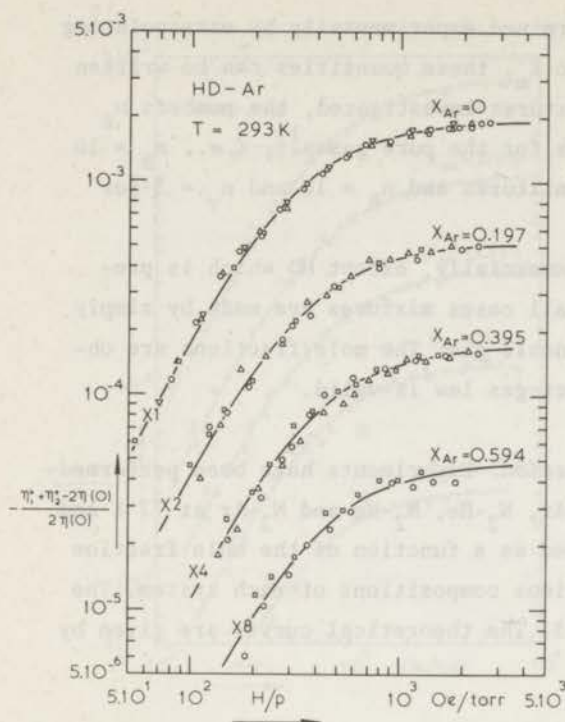


Fig. 7. $-\left[\eta_1^+ + \eta_2^+ - 2\eta(0)\right]/2\eta(0)$ versus H/p for various compositions of the system HD-Ar at 293 K.

To distinguish the different curves, they are shifted in the vertical direction as in fig. 2.

$x_{Ar} = 0$: $\circ\Delta\nabla\Box$ points taken from fig. 3.

$x_{Ar} = 0.197$: \circ 11.3 torr; Δ 16.1 torr; \Box 23.2 torr.

$x_{Ar} = 0.395$: \circ 11.4 torr; Δ 12.9 torr; \Box 18.8 torr.

$x_{Ar} = 0.594$: \circ 11.7 torr; \Box 18.3 torr.

— theoretical H/p dependence, scaled to the experimental points.

eq. (1) using ξ_{O_2} and ψ_{O_2} as adaptable parameters for the position along the H/p axis and the magnitude of the effect. It is seen that in all cases the experiments can be described very well by this theoretical expression.

4.1 The $(H/p)_{1/2}$ value as a function of composition. In figs. 14 to 17 the $(H/p)_{1/2}$ values are plotted as a function of the mole fraction of the noble gas. Within the experimental accuracy it is found that for all systems the dependence is linear, as predicted by theory [see eq. (4)]. The cross section $\xi_{(O_2A)_{AB}}^{(O_2A)}$ is obtained from the $(H/p)_{1/2}$ value extrapolated to infinite dilution of the polyatomic molecules ($x_B = 1$). In this limit the polyatomic molecules are surrounded by noble gas atoms so that reorientation occurs only through interactions of the type A-B. The values for $\xi_{(O_2A)_{AB}}^{(O_2A)}$ determined in this way are given in table II, together with $\xi(O_2)_A$ as obtained from the experiments on the pure polyatomic gas¹⁾.

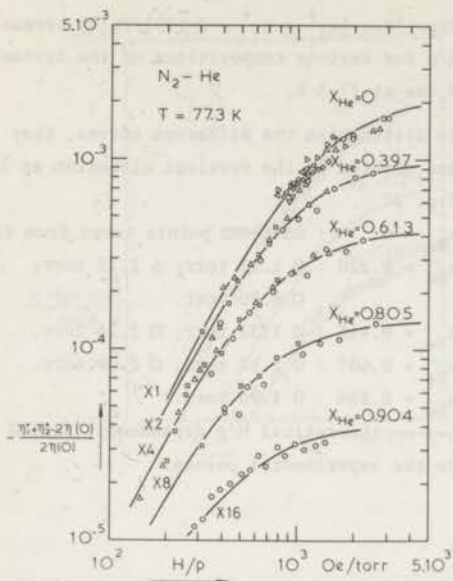


Fig. 8. $-\left[\eta_1^* + \eta_2^* - 2\eta(0)\right]/2\eta(0)$ versus H/p for various compositions of the system N_2 -He at 77.3 K.

To distinguish the different curves, they are shifted in the vertical direction as in fig. 2.

$x_{He} = 0$: \circ 0.966 torr; Δ 1.09 torr;
 \triangleright 1.72 torr; \diamond 2.04 torr;
 \triangleleft 2.48 torr; ∇ 3.29 torr;
 \square 5.08 torr.

$x_{He} = 0.397$: \circ 1.21 torr; Δ 2.19 torr;
 \square 4.02 torr.

$x_{He} = 0.613$: \circ 1.35 torr; Δ 2.06 torr;
 \square 3.94 torr.

$x_{He} = 0.805$: \circ 1.14 torr; \square 2.46 torr.

$x_{He} = 0.904$: \circ 1.98 torr.

— theoretical H/p dependence, scaled to the experimental points.

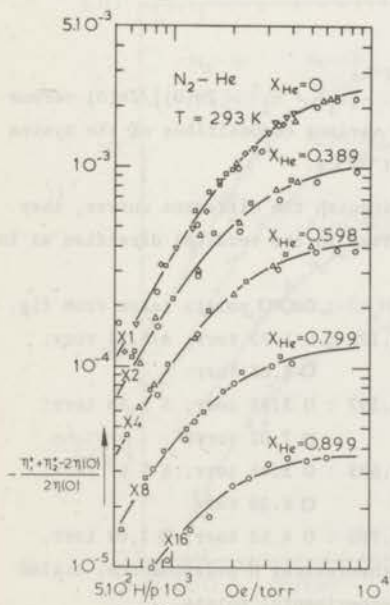


Fig. 9. $-\left[\eta_1^* + \eta_2^* - 2\eta(0)\right]/2\eta(0)$ versus H/p for various compositions of the system N_2 -He at 293 K.

To distinguish the different curves, they are shifted in the vertical direction as in fig. 2.

$x_{He} = 0$: \circ 3.61 torr; Δ 4.60 torr;
 \diamond 5.39 torr; ∇ 7.61 torr;
 \square 15.5 torr.

$x_{He} = 0.389$: \circ 3.58 torr; Δ 5.89 torr;
 \square 7.89 torr.

$x_{He} = 0.598$: \circ 3.57 torr; Δ 6.00 torr;
 \square 8.25 torr.

$x_{He} = 0.799$: \circ 6.08 torr; \square 8.75 torr.

$x_{He} = 0.899$: \circ 5.06 torr.

— theoretical H/p dependence, scaled to the experimental points.

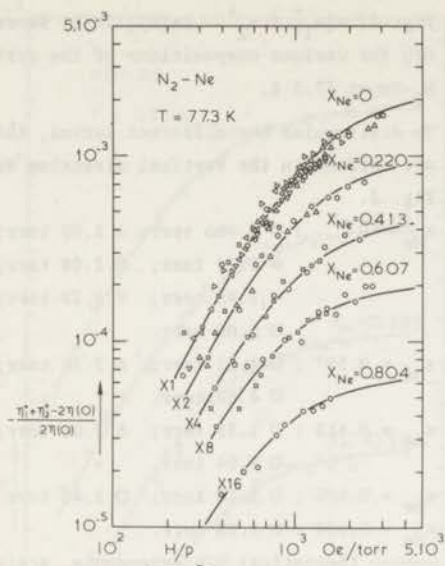


Fig. 10. $-\left[\eta_1^+ + \eta_2^+ - 2\eta(0)\right]/2\eta(0)$ versus H/p for various compositions of the system N_2-Ne at 77.3 K.

To distinguish the different curves, they are shifted in the vertical direction as in fig. 2.

$x_{Ne} = 0$: $\circ \Delta \diamond \square$ points taken from fig. 8.

$x_{Ne} = 0.220$: \circ 1.25 torr; Δ 2.13 torr;
 \square 3.80 torr.

$x_{Ne} = 0.413$: \circ 1.32 torr; \square 2.24 torr.

$x_{Ne} = 0.607$: \circ 1.13 torr; \square 2.08 torr.

$x_{Ne} = 0.804$: \circ 1.96 torr.

— theoretical H/p dependence, scaled to the experimental points.

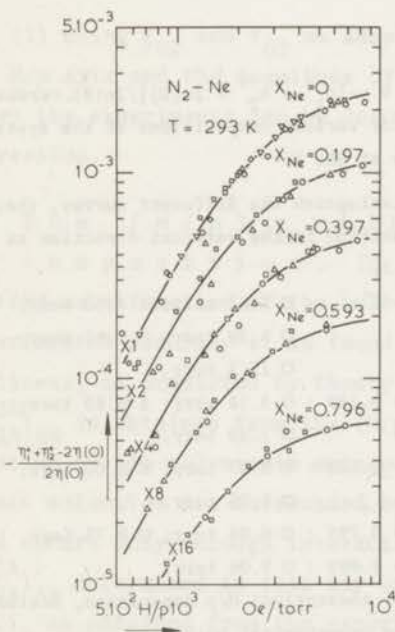


Fig. 11. $-\left[\eta_1^+ + \eta_2^+ - 2\eta(0)\right]/2\eta(0)$ versus H/p for various compositions of the system N_2-Ne at 293 K.

To distinguish the different curves, they are shifted in the vertical direction as in fig. 2.

$x_{Ne} = 0$: $\circ \Delta \diamond \square$ points taken from fig. 9.

$x_{Ne} = 0.197$: \circ 3.72 torr; Δ 5.33 torr;
 \square 8.03 torr.

$x_{Ne} = 0.397$: \circ 3.85 torr; Δ 5.16 torr;
 \square 7.02 torr.

$x_{Ne} = 0.593$: \circ 3.46 torr; Δ 5.67 torr;
 \square 8.39 torr.

$x_{Ne} = 0.796$: \circ 4.52 torr; \square 7.09 torr.

— theoretical H/p dependence, scaled to the experimental points.

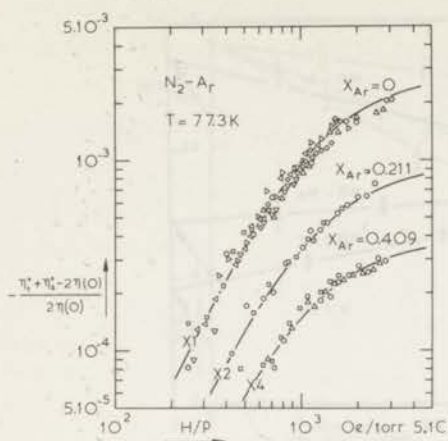


Fig. 12. $-\left[\eta_1^* + \eta_2^* - 2\eta(0)\right]/2\eta(0)$ versus H/p for various compositions of the system N_2 -Ar at 77.3 K.

To distinguish the different curves, they are shifted in the vertical direction as in fig. 2.

$x_{Ar} = 0$: \circ Δ \square points taken from fig. 8.
 $x_{Ar} = 0.211$: \circ 1.22 torr; \square 1.85 torr.
 $x_{Ar} = 0.409$: \circ 1.06 torr; Δ 1.14 torr;
 \square 1.98 torr.

— theoretical H/p dependence, scaled to the experimental points.

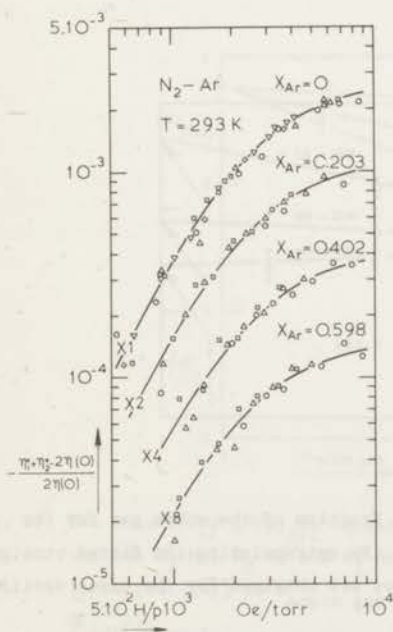


Fig. 13. $-\left[\eta_1^* + \eta_2^* - 2\eta(0)\right]/2\eta(0)$ versus H/p for various compositions of the system N_2 -Ar at 293 K.

To distinguish the different curves, they are shifted in the vertical direction as in fig. 2.

$x_{Ar} = 0$: \circ Δ \square points taken from fig. 9.
 $x_{Ar} = 0.203$: \circ 3.42 torr; Δ 5.39 torr;
 \square 7.81 torr.
 $x_{Ar} = 0.402$: \circ 3.90 torr; Δ 5.44 torr;
 \square 7.33 torr.
 $x_{Ar} = 0.598$: \circ 3.46 torr; Δ 6.23 torr;
 \square 7.42 torr.

— theoretical H/p dependence, scaled to the experimental points.

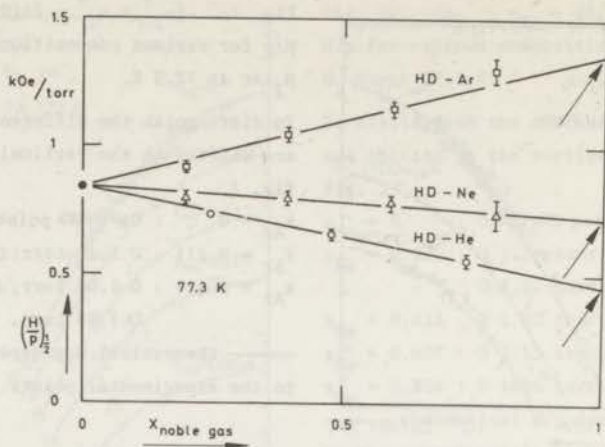


Fig. 14. The values for $(H/p)_{1/2}$ versus the mole fraction of the noble gas for the systems HD-He, HD-Ne and HD-Ar at 77.3 K. By extrapolating the fitted straight lines [eq. (4)] to $x_{\text{noble gas}} = 1$, values are obtained for the cross sections $\sigma_{(02HD)HD-n.g.}$.

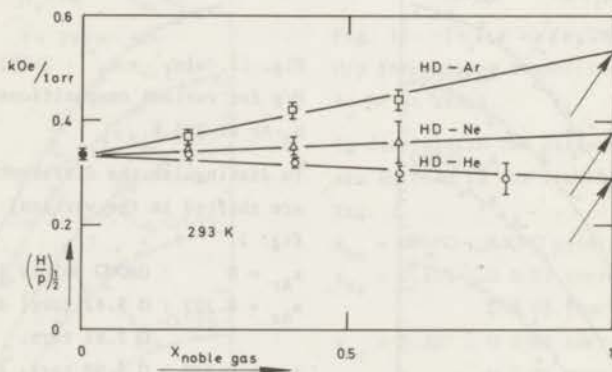


Fig. 15. The values for $(H/p)_{1/2}$ versus the mole fraction of the noble gas for the systems HD-He, HD-Ne and HD-Ar at 293 K. By extrapolating the fitted straight lines [eq. (4)] to $x_{\text{noble gas}} = 1$, values are obtained for the cross sections $\sigma_{(02HD)HD-n.g.}$.

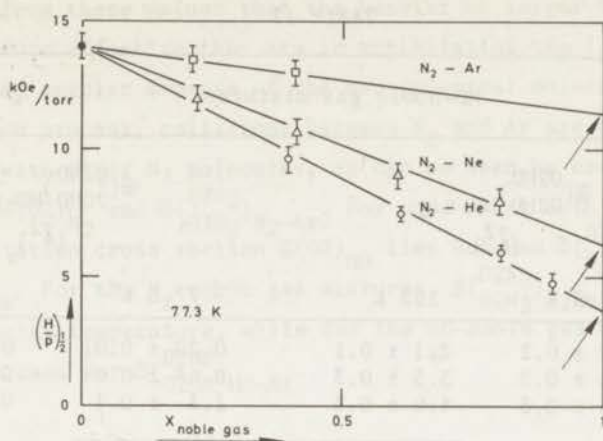


Fig. 16. The values for $(H/p)_{1/2}$ versus the mole fraction of the noble gas for the systems N_2 -He, N_2 -Ne and N_2 -Ar at 77.3 K. By extrapolating the fitted straight lines [eq. (4)] to $x_{\text{noble gas}} = 1$, values are obtained for the cross sections $\sigma_{(02N_2^2)N_2\text{-n.g.}}$.

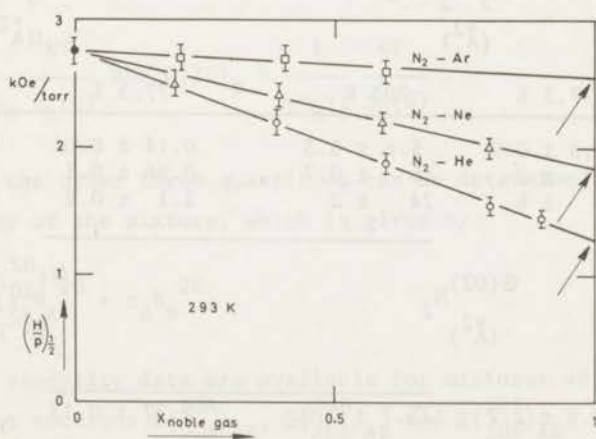


Fig. 17. The values for $(H/p)_{1/2}$ versus the mole fraction of the noble gas for the systems N_2 -He, N_2 -Ne and N_2 -Ar at 293 K. By extrapolating the fitted straight lines [eq. (4)] to $x_{\text{noble gas}} = 1$, values are obtained for the cross sections $\sigma_{(02N_2^2)N_2\text{-n.g.}}$.

TABLE II

HD-noble gas mixtures				
	$\epsilon_{(02HD)HD-n.g.}^{(02HD)}$ (\AA^2)		$\epsilon_{(20HD)HD-n.g.}^{(02HD)}$ (\AA^2)	
	77.3 K	293 K	77.3 K	293 K
HD - He	1.7 ± 0.1	2.1 ± 0.1	0.20 ± 0.01	0.14 ± 0.01
HD - Ne	3.3 ± 0.2	3.3 ± 0.3	0.65 ± 0.04	0.32 ± 0.02
HD - Ar	6.4 ± 0.3	4.9 ± 0.3	1.3 ± 0.1	0.59 ± 0.05
	$\epsilon_{(02)HD}^{(02)}$ (\AA^2)		$\epsilon_{(20)HD}^{(02)}$ (\AA^2)	
HD	2.95 ± 0.08	2.26 ± 0.07	0.519 ± 0.017	0.282 ± 0.009
N ₂ -noble gas mixtures				
	$\epsilon_{(02N_2)N_2-n.g.}^{(02N_2)}$ (\AA^2)		$\epsilon_{(20N_2)N_2-n.g.}^{(02N_2)}$ (\AA^2)	
	77.3 K	293 K	77.3 K	293 K
N ₂ - He	8.3 ± 0.9	5.6 ± 0.3	0.14 ± 0.01	0.080 ± 0.008
N ₂ - Ne	26 ± 2	15 ± 0.7	0.96 ± 0.1	0.54 ± 0.05
N ₂ - Ar	55 ± 6	24 ± 2	2.1 ± 0.2	0.98 ± 0.09
	$\epsilon_{(02)N_2}^{(02)}$ (\AA^2)		$\epsilon_{(20)N_2}^{(02)}$ (\AA^2)	
N ₂	61.9 ± 2.2	23.7 ± 0.9	2.77 ± 0.13	1.49 ± 0.05

It is seen from these values that the heavier or larger the noble gas atoms, the more effective they are in annihilating the $[J_A]^{(2)}$ polarization in the angular momenta of the non-spherical molecules. For this reorientation process, collisions between N_2 and Ar are as effective as collisions with other N_2 molecules, as can be seen by comparing the values for $\mathfrak{S}(02)_{N_2}$ and $\mathfrak{S}(02N_2)_{N_2-Ar}$. For pure HD at both temperatures the reorientation cross section $\mathfrak{S}(02)_{HD}$ lies between $\mathfrak{S}(02HD)_{HD-He}$ and $\mathfrak{S}(02HD)_{HD-Ne}$. For the N_2 -noble gas mixtures, $\mathfrak{S}(02N_2)_{N_2-n.g.}$ increases with decreasing temperature, while for the HD-noble gas mixtures this is only the case for $\mathfrak{S}(02HD)_{HD-Ar}$.

4.2. The saturation value as a function of composition.

In the theoretical expression for Ψ_{02} [see eqs. (7) and (8)] nine different cross sections occur, *viz.*, the gas-kinetic cross sections $\mathfrak{S}(20)_A$, $\mathfrak{S}(20)_B$, $\mathfrak{S}(20A)_{AB}$, $\mathfrak{S}(20B)_{AB}$ and $\mathfrak{S}(20A)_{AB}$, the reorientation cross sections $\mathfrak{S}(02)_A$ and $\mathfrak{S}(02A)_{AB}$ and the coupling coefficients $\mathfrak{S}(02)_{20A}$ and $\mathfrak{S}(02A)_{20A}$.

Of the five gas-kinetic cross sections, two are known from the field free viscosity of the pure gases, *i.e.*,

$$\mathfrak{S}(20)_A = \frac{1}{\langle v_A \rangle_0} \frac{kT}{\eta_A(0)} \quad \text{and} \quad \mathfrak{S}(20)_B = \frac{1}{\langle v_B \rangle_0} \frac{kT}{\eta_B(0)}. \quad (13)$$

In principle the other three quantities can be determined from the field free viscosity of the mixture, which is given by:

$$\eta(0) = \frac{1}{2} kT (x_A B_A^{20} + x_B B_B^{20}). \quad (14)$$

Since little viscosity data are available for mixtures we will calculate the cross sections $\mathfrak{S}(20A)_{AB}$, $\mathfrak{S}(20B)_{AB}$ and $\mathfrak{S}(20A)_{AB}$. This can be done with great accuracy as these quantities are mainly determined by the spherical part of the intermolecular interaction, so that one can relate them to the well known Ω -integrals (see *e.g.* ref. 18). Thus one gets:

$$\mathfrak{E}_{(20A)AB}^{(20A)} = \frac{8m_B}{(m_A + m_B)^2} \left\{ \frac{1}{5} m_B \Omega_{AB}^{(2,2)*} + \frac{1}{3} m_A \Omega_{AB}^{(1,1)*} \right\} \pi \sigma_{AB}^2, \quad (15)$$

$$\mathfrak{E}_{(20B)AB}^{(20B)} = \frac{8m_A}{(m_A + m_B)^2} \left\{ \frac{1}{5} m_A \Omega_{AB}^{(2,2)*} + \frac{1}{3} m_B \Omega_{AB}^{(1,1)*} \right\} \pi \sigma_{AB}^2 \quad (16)$$

and

$$\mathfrak{E}_{(20B)AB}^{(20A)} = \frac{8m_A m_B}{(m_A + m_B)^2} \left\{ \frac{1}{5} \Omega_{AB}^{(2,2)*} - \frac{1}{3} \Omega_{AB}^{(1,1)*} \right\} \pi \sigma_{AB}^2 \quad (17)$$

where $\sigma_{AB} = \frac{1}{2}(\sigma_A + \sigma_B)$ with σ_A and σ_B the Lennard-Jones diameters of molecules A and B, respectively.

The two reorientation cross sections $\mathfrak{E}(02)_A$ and $\mathfrak{E}_{(02A)AB}^{(02A)}$ have already been discussed in section 4.1 and are given in table II.

Of the two coupling cross sections $\mathfrak{E}_{(20)A}^{(02)}$ and $\mathfrak{E}_{(20A)AB}^{(02A)}$, the magnitude of the quantity $\mathfrak{E}_{(20)A}^{(02)}$ is known from experiments on the field

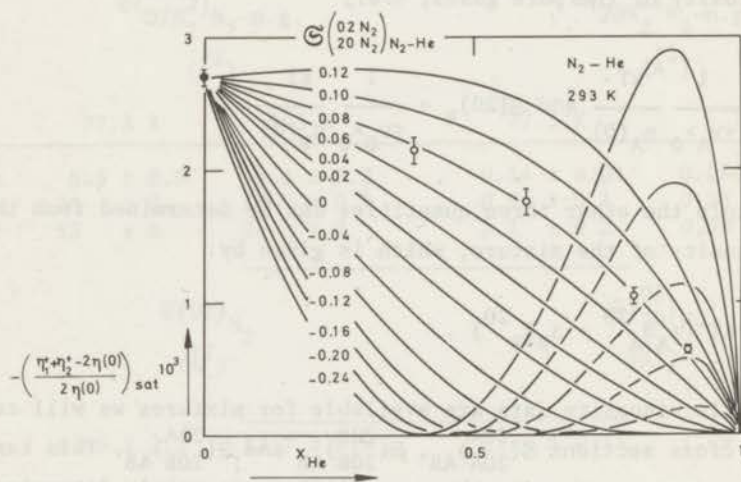


Fig. 18. The theoretical saturation values, Ψ_{02} , of $-\left[\eta_1^+ + \eta_2^+ - 2\eta(0)\right]/2\eta(0)$ versus the mole fraction of He for the system N_2 -He at 293 K, calculated from eq. (7) for various values of $X_{(02N_2)_{20N_2}^{(02N_2)_{20N_2}}}$. The best agreement with the experimental points is found for $X_{(02N_2)_{20N_2}^{(02N_2)_{20N_2}}} = +0.08 \text{ \AA}^2$.

effect in pure gases, while the sign can be determined from measurements on streaming birefringence. Such experiments have been performed for N_2 ¹⁹⁾ and recently also for HD²⁰⁾. In both cases the sign is found to be positive. The cross section $\mathfrak{E}_{(20A)AB}^{(02A)}$ is the only remaining quantity in eq. 7 which is not yet known and is therefore determined from the experiments reported here. Fig. 18 gives the theoretical curves and experimental points for the saturation value Ψ_{02} as a function of noble gas mole fraction. The theoretical curves are calculated with various values of $\mathfrak{E}_{(20N_2)N_2-He}^{(02N_2)}$ both positive and negative. It is obvious that good agreement between theory and experiment can be obtained for $\mathfrak{E}_{(20N_2)N_2-He}^{(02N_2)} = + 0.080 \text{ \AA}^2$. Note that eq. 7 gives the same results if the sign of both $\mathfrak{E}_{(20)N_2}^{(02)}$ and $\mathfrak{E}_{(20N_2)N_2-He}^{(02N_2)}$ is changed, because of the square in the numerator so that in fact one can conclude from our experiments that both coupling cross sections have the same sign. For all mixtures such plots are made and always good agreement between theory and experiment is found for a given value of $\mathfrak{E}_{(20A)AB}^{(02A)}$. Moreover, the sign of $\mathfrak{E}_{(20A)AB}^{(02A)}$ is always the same as that of $\mathfrak{E}_{(20)A}^{(02)}$. In figs. 19 to 22 the results for all investigated systems are shown, along with the theoretical curve which gives best agreement with the experimental data. The various parameters used in these calculations were obtained from refs. 21 to 24 and are summarized in table III. In table II

TABLE III

Summary of the parameters used in the calculations				
	ϵ/k	σ	$\eta(0)$	
	(K)	(\AA)	(μP)	
			77.3 K	293 K
He	10.22	2.556	83	196
Ne	34.9	2.780	120	312
Ar	119.8	3.405	66	223
HD	37.0	2.928	42	107
N_2	91.5	3.681	54	174

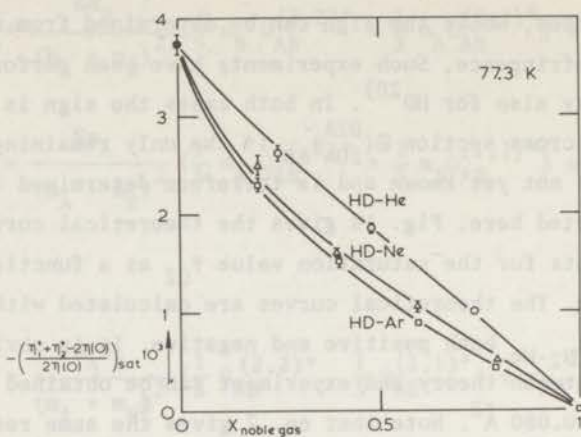


Fig. 19. The saturation values of $-\left[\eta_1^+ + \eta_2^+ - 2\eta(0)\right]/2\eta(0)$ versus the mole fraction of the noble gas for the systems HD-He, HD-Ne and HD-Ar at 77.3 K. The solid lines are given by eq. (7) using the value of $\mathcal{E}_{(20HD)}^{(02HD)}_{HD-n.g.}$ which gives the best fit of the experimental points.

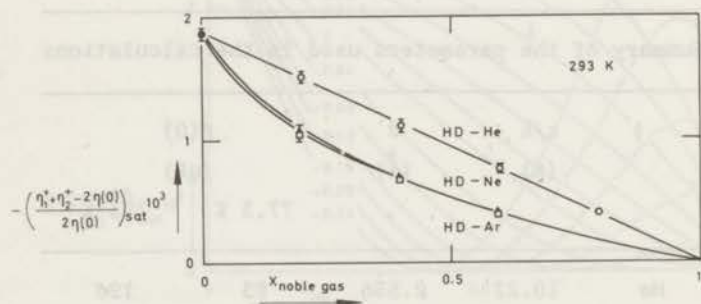


Fig. 20. The saturation values of $-\left[\eta_1^+ + \eta_2^+ - 2\eta(0)\right]/2\eta(0)$ versus the mole fraction of the noble gas for the systems HD-He, HD-Ne and HD-Ar at 293 K. The solid lines are given by eq. (7) using the value of $\mathcal{E}_{(20HD)}^{(02HD)}_{HD-n.g.}$ which gives the best fit of the experimental points.

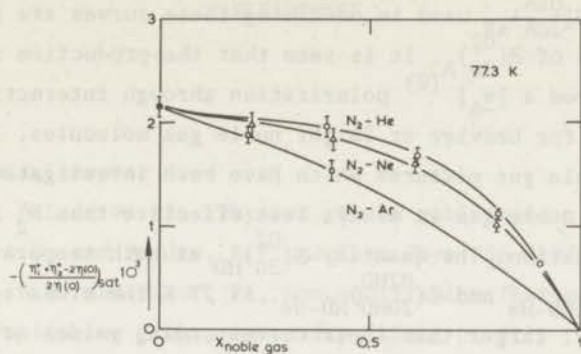


Fig. 21. The saturation values of $-\left[\eta_1^+ + \eta_2^+ - 2\eta(0)\right]/2\eta(0)$ versus the mole fraction of the noble gas for the system N_2 -He, N_2 -Ne and N_2 -Ar at 77.3 K. The solid lines are given by eq. (7) using the value of $\Theta_{(02N_2)N_2-n.g.}$ which gives the best fit of the experimental points.

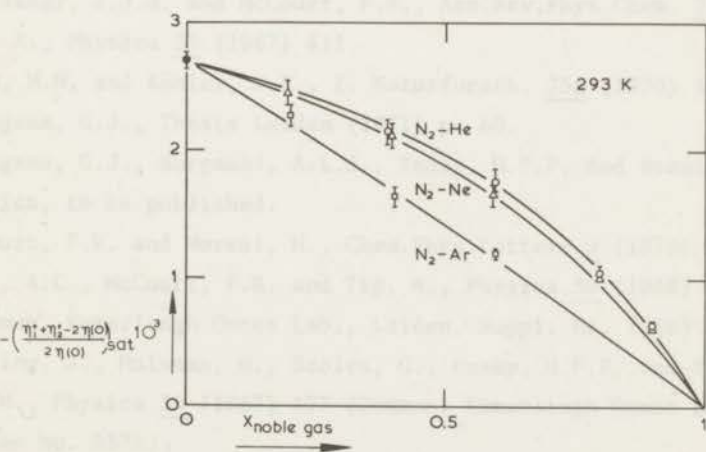
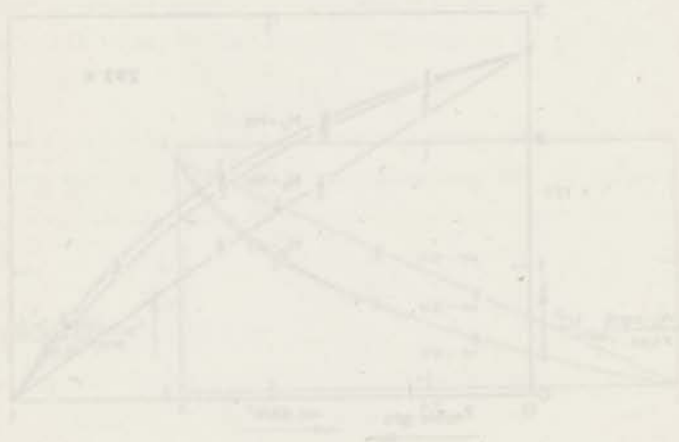


Fig. 22. The saturation values of $-\left[\eta_1^+ + \eta_2^+ - 2\eta(0)\right]/2\eta(0)$ versus the mole fraction of the noble gas for the system N_2 -He, N_2 -Ne and N_2 -Ar at 293 K. The solid lines are given by eq. (7) using the value of $\Theta_{(20N_2)N_2-n.g.}$ which gives the best fit of the experimental points.

the values of $\mathfrak{E}_{(20A)AB}^{(02A)}$ used in obtaining these curves are given together with the values of $\mathfrak{E}_{(20)A}^{(02)}$. It is seen that the production of $[J_A]^{(2)}$ polarization from a $[W_A]^{(2)}$ polarization through interactions A-B is more effective for heavier or larger noble gas molecules. In all the cases of N_2 -noble gas mixtures which have been investigated, it is found that the noble gas is always less effective than N_2 in producing $[J_A]^{(2)}$ polarization. The quantity $\mathfrak{E}_{(20)HD}^{(02)}$ at both temperatures lies between $\mathfrak{E}_{(20HD)HD-He}^{(02HD)}$ and $\mathfrak{E}_{(20HD)HD-Ne}^{(02HD)}$. At 77 K the cross sections $\mathfrak{E}_{(20A)AB}^{(02A)}$ are all larger than their corresponding values at 293 K, while the relative increase with temperature is larger for heavier noble gas molecules.



REFERENCES

1. This thesis, chapter I.
Burgmans, A.L.J. *et al.*, Physica, to be published.
2. Coope, J.A.R. and Snider, R.F., J.Chem.Phys. 56 (1972) 2056.
3. De Groot, S.R. and Mazur, P., Non-equilibrium Thermodynamics, (North-Holland Publishing Comp., Amsterdam, 1962) p. 311.
4. Moraal, H., McCourt, F.R. and Knaap, H.F.P., Physica 45 (1969) 455
(Commun. Kamerlingh Onnes Lab., Leiden, Suppl. No. 127d).
5. Hulsman, H. and Burgmans, A.L.J., Phys. Letters 29A (1969) 629.
6. Hulsman, H., van Waasdijk, E.J., Burgmans, A.L.J., Knaap, H.F.P.
and Beenakker, J.J.M., Physica 50 (1970) 53 (Commun. Kamerlingh
Onnes Lab., Leiden No. 381e).
7. Hulsman, H., van Kuik, F.G., Walstra, K.W., Knaap, H.F.P. and
Beenakker, J.J.M., Physica 57 (1972) 501 (Commun. Kamerlingh Onnes
Lab., Leiden No. 389a).
8. Korving, J., Physica, to be published.
9. Beenakker, J.J.M. and McCourt, F.R., Ann.Rev.Phys.Chem. 21 (1970) 47.
10. Tip, A., Physica 37 (1967) 411.
11. Raum, H.H. and Köhler, W.E., Z. Naturforsch. 25a (1970) 1178.
12. Prangmsma, G.J., Thesis Leiden (1971) p. 60.
Prangmsma, G.J., Burgmans, A.L.J., Knaap, H.F.P. and Beenakker, J.J.M.,
Physica, to be published.
13. McCourt, F.R. and Moraal, H., Chem.Phys.Letters 9 (1971) 39.
14. Levi, A.C., McCourt, F.R. and Tip, A., Physica 39 (1968) 165
(Commun. Kamerlingh Onnes Lab., Leiden, Suppl. No. 126b).
15. Korving, J., Hulsman, H., Scoles, G., Knaap, H.F.P. and Beenakker,
J.J.M., Physica 36 (1967) 177 (Commun. Kamerlingh Onnes Lab.,
Leiden No. 357b).
16. Loeb, L.B., The kinetic theory of gases (McGraw Hill Book Cy., Inc.
New York and London, 1934) p. 297.
17. Chapman, S. and Cowling, T.G., The mathematical theory of non-uniform
gases, (Cambridge University Press, 1970). p. 88.

18. Chapman, S. and Cowling, T.G., The mathematical theory of non-uniform gases, (Cambridge University Press, 1970). p. 159.
19. Baas, F., Phys. Letters 36A (1971) 107.
20. Baas, F., private communication.
21. Hirschfelder, J.O., Curtiss, C.F. and Bird, R.B., The molecular theory of gases and liquids, (John Wiley and Sons, Inc. New York, 1954) p. 1110.
22. Data Book, edited by Thermophysical Properties Research Center, Purdue University (Lafayette, Indiana, 1966) Vol. 2.
23. Rietveld, A.O., Van Itterbeek, A., Velds, C.A., Physica 25 (1959) 205 (Commun. Kamerlingh Onnes Lab., Leiden No. 314b).
24. Rietveld, A.O. and Van Itterbeek, A., Physica 22 (1956) 785 (Commun. Kamerlingh Onnes Lab., Leiden No. 304e).

SAMENVATTING

De moleculaire snelheden \underline{W} in een gas zijn niet meer isotroop verdeeld, zodra er in dat gas een gradient wordt aangelegd in bijvoorbeeld de temperatuur of de driftsnelheid. Een dergelijke polarisatie in de snelheden geeft aanleiding tot transport van energie c.q. impuls. In een gas van meeratomige moleculen is de situatie echter veel ingewikkelder, daar in dat geval door middel van botsingen polarisaties kunnen worden opgebouwd die afhankelijk zijn van het impulsmoment \underline{J} . Tengevolge van een gradiënt in de driftsnelheid (viscositeitsexperimenten) ontstaat een polarisatie in de \underline{W} ruimte van het quadrupool type $\langle [\underline{W}]^{(2)} \rangle$, en wordt er door botsingen een polarisatie in de \underline{J} ruimte opgebouwd van het type $\langle [\underline{J}]^{(2)} \rangle$.

Indien een uitwendig magneetveld wordt aangelegd, zullen de impulsmomenten een precessie om de veldrichting gaan uitvoeren, hierdoor zal de $\langle [\underline{J}]^{(2)} \rangle$ polarisatie voor een deel teniet worden gedaan. Dit geeft vervolgens aanleiding tot een afname van de $\langle [\underline{W}]^{(2)} \rangle$ polarisatie, waardoor de viscositeit verandert. Uit dit viscomagnetisch effect kan informatie worden verkregen over de sterkte van de koppeling tussen de polarisaties in de \underline{W} en \underline{J} ruimten en over de snelheid waarmee de $\langle [\underline{J}]^{(2)} \rangle$ polarisatie vervalst. Deze grootheden worden voornamelijk bepaald door het niet-bolvormige deel van de intermoleculaire potentiaal. Een studie van het viscomagnetisch effect opent daarom de mogelijkheid om het niet-bolvormige deel van de moleculaire wisselwerking te onderzoeken.

Bij de aanvang van het in dit proefschrift beschreven onderzoek waren vrijwel alle metingen die aan het viscomagnetisch effect waren verricht, uitgevoerd bij kamertemperatuur. Om informatie over het niet-bolvormige deel van de moleculaire wisselwerking te verkrijgen is het echter noodzakelijk over gegevens te beschikken in een groot temperatuurgebied. De resultaten die verkregen zijn voor HD, N_2 , CO en CH_4 bij temperaturen tussen 293 K en het kookpunt van het betreffende gas worden gegeven in hoofdstuk I.

Informatie over het verval van polarisaties in de J ruimte kan eveneens worden verkregen uit metingen aan kernspin relaxatie (N.M.R.) in verdunde gassen. Een vergelijking tussen de resultaten van het visco-magnetisch effect en die van N.M.R. metingen wordt eveneens gegeven in hoofdstuk I.

Aangezien de beschrijving van het botsingsproces tussen twee meer-atomige moleculen zeer gecompliceerd is, is het uit theoretisch oogpunt zinnig ook te beschikken over metingen aan mengsels van meeratomige gasen met edelgassen. Daarom zijn er metingen verricht aan de systemen HD-He, HD-Ne, HD-Ar, N_2 -He, N_2 -Ne en N_2 -Ar bij zowel 77 K als 293 K. De resultaten hiervan worden gegeven in hoofdstuk II. Voor al deze systemen bleek een goede overeenkomst te bestaan tussen theorie en experiment.

CURRICULUM VITAE

Op verzoek van de faculteit der Wiskunde en Natuurwetenschappen volgen hier enige gegevens over mijn studie.

Na mijn H.B.S.-B opleiding van 1957 tot 1962 aan het Sint Odulphuslyceum te Tilburg begon ik in september 1962 mijn studie aan de Rijksuniversiteit te Leiden, waar ik in 1966 het kandidaatsexamen Natuurkunde en Wiskunde met als bijvak Sterrekunde aflegde. Sindsdien ben ik werkzaam op het Kamerlingh Onnes Laboratorium in de werkgroep voor Moleculfysica onder leiding van Prof. Dr. J.J.M. Beenakker en Dr. H.F.P. Knaap. Aanvankelijk assisteerde ik Drs. I.N. Bakx bij haar onderzoek betreffende de mengwarmte van de systemen $\text{OH}_2\text{-PH}_2$ en $\text{OD}_2\text{-PD}_2$ in de vloeistoffase. Vervolgens heb ik deelgenomen aan het onderzoek van Dr. J.P. Brouwer naar de soortelijke warmte van de vloeistofmengsels Ne-H_2 en Ne-D_2 in het ontmenggebied. Vanaf begin 1968 assisteerde ik Dr. H. Hulsman bij zijn onderzoek aan het dwars-impulstransport in meeratomige gassen onder invloed van een magneetveld. In 1969 legde ik het doctoraalexamen Natuurkunde af en begon aan het in dit proefschrift beschreven onderzoek.

In 1968 werd ik assistent op het natuurkundig practicum, aanvankelijk voor studenten in de Geneeskunde en later voor studenten met als hoofdvak Natuurkunde.

Het in dit proefschrift beschreven onderzoek werd voor een belangrijk deel verricht in samenwerking met Drs. P.G. van Ditzhuyzen, terwijl ik in verschillende stadia van het experimentele werk achtereenvolgens werd geassisteerd door A.H. Alberga, Drs. S.P. van Dijk en B.J. Thijsse. Dr. J. Korving ben ik zeer erkentelijk voor het beschikbaar stellen van een aantal theoretische beschouwingen aangaande het viscomagnetische effect voor mengsels.

De constructie van de apparaten, nodig voor het onderzoek werd uitgevoerd door de heren J.M. Verbeek en P. Zwanenburg. Een aantal technische voorzieningen kwamen tot stand dankzij de inspanningen van ver-

STELLINGEN

I

Metingen aan gedepolariseerde Rayleigh lichtverstrooiing zijn bijzonder geschikt om na te gaan of de botsingsdoorsnede voor reoriëntatie van het impulsmoment van twee-atomige moleculen afhangt van de rotatietoestand van het molecuul.

II

De minima die voorkomen in de isentropen van $\text{Cu}(\text{NO}_3)_2 \cdot 2\frac{1}{2}\text{H}_2\text{O}$ worden door Haseda *et al.* gezien als gevolg van een faseovergang tussen de paramagnetische en de antiferromagnetische toestand, dit is echter onjuist.

Haseda, T., Tokunaga, Y., Yamada, R.,
Kuramitsu, Y., Sakatsume, S., Amaya, K.,
Proc. 12th Int. Conf. on low Temp. Phys.,
Kyoto (1970) 685.

III

Speight en Armstrong houden in de analyse van de kernspin relaxatie metingen aan N_2 ten onrechte geen rekening met het voorkomen van ortho en para modificaties.

Speight, P.A. and Armstrong, R.L., Canad.J.
Phys., 47 (1969) 1475.

IV

Aangezien Powell en Hildebrand bij de interpretatie van metingen aan de diffusie van gassen in vloeistoffen gebruik maken van het kritische volume, zijn hun conclusies twijfelachtig.

Powell, R.J. en Hildebrand, J.H., J.Chem. Phys., 55 (1971) 4715.

V

De wijze waarop Atkins in zijn boek Molecular Quantum Mechanics de spinrotatie koppeling van het zuurstofmolecuul behandelt is onjuist.

Atkins, P.W., Molecular Quantum Mechanics, (Oxford University Press, 1970) p. 337.

VI

Het is bedrieglijk de isotopische onzuiverheid van stoffen als ND_3 en CD_4 op te geven in het aanwezige percentage waterstof atomen.

VII

Om "kritische toestand" modellen voor irreducibele type II supergeleiders te testen, is de methode waarbij de fluxgradiënt als functie van de inductie wordt bepaald uit de gemeten magnetisatie, geschikter dan de methode waarbij de magnetisatie aan de hand van deze modellen wordt berekend.

Campbell, A.M., Evetts, J.E. en Dew-Hughes, D., Phil.Mag., 18 (1968) 313.
Kes, P.H., Van der Klein, C.A.M. en De Klerk, D., nog te publiceren.

VIII

De symmetrie van het CH_4 molecuul heeft tot gevolg dat het niet gerechtvaardigd is bij lage temperaturen de uitdrukking $\langle I^2 J^2 \rangle$ te vervangen door $\langle I^2 \rangle \langle J^2 \rangle$, (I is de totale kernspin en J het impulsmoment).

IX

De elektrische polariseerbaarheid wordt in het MKSA stelsel uitgedrukt in m^3 en in het CGS stelsel in cm^3 , zodat de omrekeningsfactor $4\pi \times 10^6$ bedraagt.

X

Het onderscheid tussen snelverkeer en langzaam verkeer heeft gezien de verkeerssituatie in de meeste grote steden veel van zijn oorspronkelijke betekenis verloren.

Leiden, 20 september 1972

A.L.J. Burgmans

The system is based on the principle of the
 least squares method. It is a
 method of determining the best
 fit of a set of data points.

The method is based on the
 principle of the least squares
 method. It is a method of
 determining the best fit of a
 set of data points.

11

The method is based on the
 principle of the least squares
 method. It is a method of
 determining the best fit of a
 set of data points.

The method is based on the
 principle of the least squares
 method. It is a method of
 determining the best fit of a
 set of data points.

The method is based on the
 principle of the least squares
 method. It is a method of
 determining the best fit of a
 set of data points.

The method is based on the
 principle of the least squares
 method. It is a method of
 determining the best fit of a
 set of data points.

The method is based on the
 principle of the least squares
 method. It is a method of
 determining the best fit of a
 set of data points.

12

The method is based on the
 principle of the least squares
 method. It is a method of
 determining the best fit of a
 set of data points.

The method is based on the
 principle of the least squares
 method. It is a method of
 determining the best fit of a
 set of data points.

scheidene leden van de vaste staf van het Kamerlingh Onnes Laboratorium, met name de heren J. Turenhout, J. Dunsbergen en T.A. van der Heijden. De tekeningen van dit proefschrift zijn verzorgd door de heer J.A.J.M. Disselhorst. Mej. A.M. Aschoff zorgde op voortreffelijke wijze voor het uittypen van het manuscript. De Engelse tekst werd gecorrigeerd door Dr. B.C. Sanctuary. De heer W.F. Tegelaar verzorgde de foto's en de omslag van dit proefschrift.

gelyken (ook van de vrees niet van het karmisch Guna-laboratorium
 met name de naam J. Tuschner, A. Bamberger en T. A. van der Heijden.
 De tekeningen van dit proefschied zijn verspreid door de heer J. J. M.
 Hasselhorst, W. J. A. M. Scholtz, J. G. van der Heijden, J. G. van der
 Heijden, van het ministerie. De laatste teken is verspreid door
 Dr. J. C. Bamberger, de heer W. J. Tuschner, verspreid de foto's en de te-
 kening van dit proefschied.

